Research and Development on Critical (Sonic) Flow of Multiphase Fluids through Wellbores in Support of Worst-Case-Discharge Analysis for Offshore Wells

Mewbourne School of Petroleum and Geological Engineering
The University of Oklahoma, Norman
100 E Boyd St. Norman, OK-73019

The UNIVERSITY of OKLAHOMA

October 2, 2018

This page intentionally left blank.

Research and Development on Critical (Sonic) Flow of Multiphase Fluids through Wellbores in Support of Worst-Case-Discharge Analysis for Offshore Wells

Authors:

Saeed Salehi, Principal Investigator
Ramadan Ahmed, Co- Principal Investigator
Rida Elgaddafi, Postdoctoral Associate
Olawale Fajemidupe, Postdoctoral Associate
Raj Kiran, Research Assistant

Report Prepared under Contract Award M16PS00059
By: Mewbourne School of Petroleum and Geological Engineering
The University of Oklahoma, Norman

For: The US Department of the Interior
Bureau of Ocean Energy Management Gulf of Mexico OCS Region

This page intentionally left blank.

DISCLAIMER

Study concept, oversight, and funding were provided by the US Department of the Interior, Bureau of Ocean Energy Management (BOEM), Environmental Studies Program, Washington, DC, under Contract Number M16PS00059. This report has been technically reviewed by BOEM, and it has been approved for publication. The views and conclusions contained in this document are those of the authors and should not be interpreted as representing the opinions or policies of the US Government, nor does mention of trade names or commercial products constitute endorsement or recommendation for use.

Table of Contents

List of Figures

List of Tables

Nomenclature

Abbreviations and Acronyms

Symbol	Description	Units
A	Cross-section area of pipe	m^2
B_g	Gas formation volume factor	ft^3/scf
B_o	Oil formation volume factor	bbl/STB
$\overline{B}_o$	Average oil formation volume factor	bbl/STB
B_{ob}	Oil formation volume factor at bubble point pressure	bbl/STB
B_w	Water formation volume factor	bbl/STB
$\overline{B}_w$	Average water formation volume factor	bbl/STB
C	Constant factor relating friction factor to Reynolds number for smooth pipes	-
c_o	Isothermal compressibility	psi^{-1}
d	Pipe diameter	m
D	Deposition rate	m3/s
f	Friction factor	-
F_E	Fraction of liquid entrained in gas core	-
g	Gravity acceleration	m/s^2
h	Thickness of producing gas layer	ft
H	Average holdup fraction	-
J_o	Oil productivity index	STD/d/psi
J_w	Water productivity index	STD/d/psi
k	absolute permeability	md
k_o	Oil permeability	md
k_{rg}	Relative gas permeability	-
k_{ro}	Relative oil permeability	-
k_{rw}	Relative water permeability	-
k_w	Water permeability	md
M	Molecular weight	lb/mol
M_a	Apparent molecular weight for gas	lb/lbmol
N_{Re}	Reynolds number	-
r_e	Reservoir radius	ft/m
r_w	Well-bore radius	ft/m
R	Gas universal constant	$10.730\ \frac{psia.ft^3}{lbmol\ °R}$
R_s	Solution gas oil ratio	scf/STB
P	Pressure	psia or Pa
$\overline{P}$	Average pressure	psia or Pa

P_b	Bubble point pressure	psia or Pa
P_r	Reservoir pressure	psia or Pa
P_{wf}	Well bore flowing pressure	psia or Pa
PI	Productivity index	STD/d/psi
q	Flowrate	m^3/s
q_s	Production flowrate	STB/d
$q_{g_{STB}}$	Gas flowrate at stock tank barrel	scf/d
$q_{g(uncon)}$	Un-condensate gas rate	scf/d
q_o	Oil production rate	STD/d
q_{STW}	Water production rate at stock tank	STB/d
q_W	Water production rate	STD/d
S	Wetted perimeter	m
S_k	Skin factor	-
S_g	Gas saturation	%
S_{gc}	Critical gas saturation	%
S_o	Oil saturation	%
S_o^*	Effective oil saturation	%
S_{oc}	Critical oil saturation	%
S_w	Water saturation	%
S_{wc}	Critical water saturation	%
S_{wi}	Irreducible water saturation	
T	Temperature	
v	Velocity	m/s
V	Volume	m^3
W	Solid angle related with the deposition area	
X	Lockhart and Martinelli parameter	-
X_M	Modified Lockhart and Martinelli parameter	-
Y	Lockhart and Martinelli parameter	-
Y_M	Dimensionless group	-
Z	Empirical factor defining interfacial friction	-
$\overline{Z}_f$	Gas compressibility factor	-

Greek Symbol

Symbol	Description	Units
β	Length ratio defined	-
δ	Film thickness	m
$\underline{\delta}$	Ratio of film thickness to diameter	-
ε	Absolute pipe roughness	m

λ	No-slip holdup fraction	-
ν	Kinematic viscosity	m^2/sq
ρ	Density	kg/m^3
σ	Surface tension	dyne/cm
τ	Shear stress	N/m^3
ϕ	Dimensionless groups	-
α	Void Fraction	-
γ_g	Gas specific gravity	-
γ_o	Oil specific gravity	-
μ	Dynamic viscosity	kg/m.s
μ_g	Gas Viscosity	kg/m.s
$\overline{\mu_g}$	Average gas viscosity	kg/m.s
μ_{ob}	Oil viscosity at bubble point pressure	kg/m.s
μ_{oD}	Viscosity of the dead oil	kg/m.s
μ_w	Water viscosity	kg/m.s

Subscripts and Superscript

Symbol	**Description**
*	Developing slug flow
a	Acceleration
A	average
c	Taylor bubble cap, Core
Ca	Casing
crit	Critical
d	Dimensionless
e	Elevation
f	friction
F	Film
g	gas
H	Hydraulic
i	ith element
I	Interfacial
L	Liquid
LS	Liquid slug
m	Mixture
M	Modified
max	Maximum
min	Minimum
N	Nusselt
p	pipe
r	Relative
s	Slip

S	Superficial
SU	Slug unit
t	Total
TB	Taylor bubble
TP	Two-phase
Tu	Tubing

Executive Summary

This report presents a comprehensive computational tool for high Mach number (0.3 – 1+ Mach) flow WCD estimation. The tool was developed at the University of Oklahoma under BSEE/BOEM project no. M16PS00059. The report includes: i) a brief introduction describing the importance of investigating WCD scenario and objectives that have been set for this study; ii) theory and WCD tool formulation, and iii) validation of hydrodynamic flow mechanistic models incorporated in the WCD tool. The second section presents in details the WCD – tool components, which is consisted of: i) nodal analysis; ii) PVT models; iii) production models; and iv) hydrodynamic flow models. Finally, the third section presents the comparison of pressure gradient predictions for single and two-phase flow in a vertical pipe with experimental data obtained from OU – Lab and other existing studies. The model performance was tested under various test wellbore conditions, which are considered as key factors affecting WCD rate. During the validation study, test variables including pipe sizes, superficial gas, and liquid velocities, flow patterns, and inclination angle were varied.

Accurate prediction of WCD scenario is strongly related to the accuracy of the two-phase flow model. During WCD computational tool development, different two-phase flow mechanistic and empirical models were tested to describe pressure profile along the wellbore with various flow patterns. It is noteworthy that these models were basically developed for low superficial gas velocity application and their performance has never been tested for high superficial gas and liquid velocities. Thus, high-velocity pressure gradient measurement obtained from the multiphase flow loop at University of Oklahoma was utilized to validate these models. As a result, two models (Hasan and Kabir; Ansari) were adopted for different flow patterns including bubble, low-velocity slug, high-velocity slug, and annular flow. High-velocity slug and annular flow models were modified to suit the purpose of Worst-Case Discharge (WCD) estimation. Furthermore, a new boundary criterion for the application of these models was established based on the consensus of their predictions with OU – Lab data. In this study, new hybrid models for low and high-velocity slug flow, as well as a high-velocity slug and annular flow, were developed. A sonic model was developed based on the existing models available in the literature. Good agreement was obtained between model predictions of sonic velocity and OU – lab measurement.

One of the project findings is that WCD rate is not only reliant on conditions of the wellbore section but it is also influenced by the fluid properties and reservoir characteristics. Therefore, the developed WCD tool accounts for different reservoir types with the characteristics including up to 15 producing layers, reservoir formation (consolidated and unconsolidated), fluid types (oil, gas water, and gas condensate), and thickness of the pay zone. In addition, the tool allows the user to specify fluid and reservoir properties for each layer including permeability, water, oil and gas saturation, API gravity of oil, salt concentration, bubble point and reservoir pressure, irreducible water saturation, critical oil and gas saturation, and gas specific gravity. With respect to wellbore section, the tool provides flexible options for the user to design the desired wellbore configuration. These options comprise of postulating the depth of cased and open-hole sections, casing and hole diameter, roughness of casing and open-hole section and the

inclination angle of the wellbore. It is noteworthy that the tool provides a good WCD prediction up to 45° from the vertical level.

Finally, a comprehensive WCD Computational tool is developed based on mechanistic models and experimental data measured at the University of Oklahoma. As outputs, the tool predicts WCD rate, gas and water rate, the occurrence of the sonic condition and surface pressure. In addition, it provides an inflow performance relationship (IPR curves) for each reservoir layer. The accuracy of the modified mechanistic models was tested and validated with the data acquired from the OU – Lab experiments. The performance of the model is in good agreement with experimental data, which in the end provides a strong confidence in WCD rate predictions.

1. Introduction

1.1 Background

Worst Case Discharge (WCD) because of a blowout is a major concern in the oil and gas industry. An uncontrolled release of fluids from the reservoir into the wellbore, known as blowout may occur during drilling operations. In order to estimate the daily rate of uncontrolled release of fluid from the reservoir to the wellbore, an accurate predictive model is necessary. Furthermore, generalized models such as empirical and analytical cannot extensively address complex physical phenomena of multiphase flow. To solve this kind of complex riddles mechanistic model is required. This type of models solves the combined momentum balance equations for each phase. Continuity is preserved by applying simultaneous mass balances of the phases.

Based on these reasons, an extensive mechanistic model for high Mach number (0.3 – 1+ Mach) flow on WCD calculation has been developed. The mechanistic model consists of sub-models for flow pattern, pressure gradient and estimation of Worst-Case Discharge (WCD). The comprehensive model is examined and validated using experimental results for high Mach number (0.3 – 1+ Mach) flow. The experimental data were acquired from the setup designed and constructed for this purpose in Well Construction and Technology Centre (WCTC) of the Department of Petroleum Engineering at the University of Oklahoma.

1.2 Objectives

The primary objective of this report is to develop a user-friendly computational tool to estimate Worst-Case-Discharge under realistic and various conditions existing in wellbores. Additionally, this work is aimed to attain other principal objectives, which are listed as follows:

- A better understanding of physical phenomena associated with WCD scenario, particularly behavior of two-phase flow at a high Mach number.

- Developing a mechanistic model to predict single and two-phase flow characteristics for different WCD scenarios in the wellbore at a high Mach number.

- Integrate various models such as PVT fluid properties models, production models, and reservoir performance models to accurately describe the fluid flowing from the reservoir through the wellbore and ultimately predict the WCD rate.

- Investigate the influence of multi- producing layers and wellbore inclination angle on WCD estimation.

2. Theory and Tool Formulation

2.1 WCD Model Description

After the Gulf of Mexico (GOM) crisis, an estimation of Worst-Case Discharge rate becomes a requirement from the Bureau of Ocean Energy Management (BOEM) prior to all wells being permitted in the GOM. Therefore, development of precision WCD model is the main objective of this project. Accurate WCD model accounts for the relevant reservoir and wellbore characteristics and fluid properties without ignoring the possible real scenario. A comprehensive WCD model formulated by combining the inflow and outflow models to predict WCD rate, and profiles of superficial velocities, pressure and various flow patterns along the wellbore. The schematic of WCD-computation tool components is depicting in **Figure 2.1**

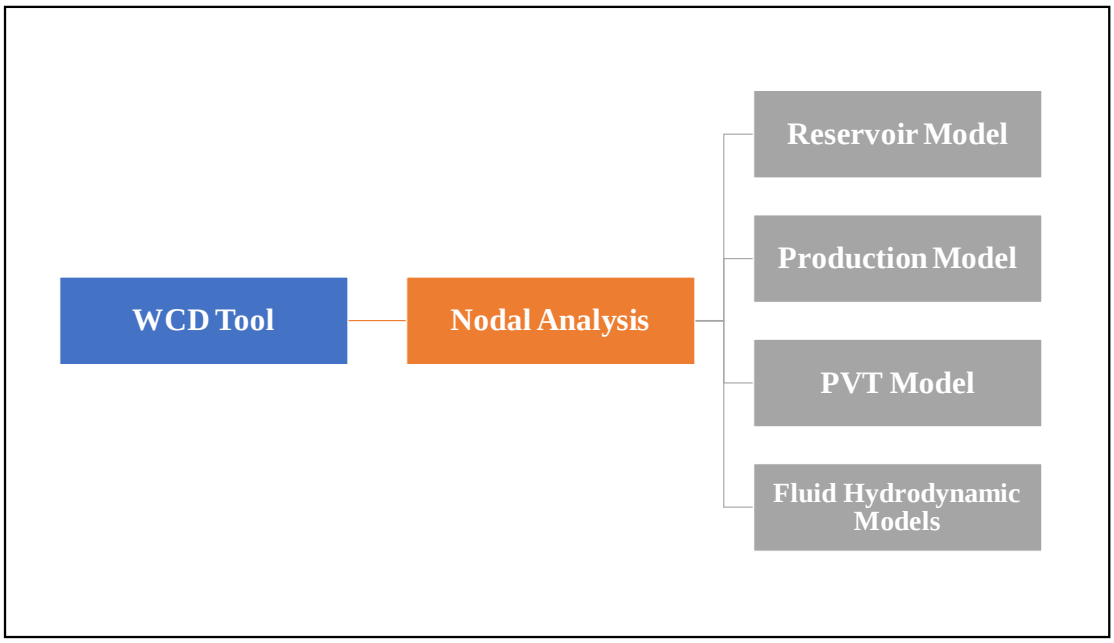

Figure 2.1 Schematic of WCD – Computation Tool Components

2.2 Nodal Analysis

In petroleum production engineering, nodal analysis is a relationship between the inflow performance relationship (IPR) and the vertical lift performance (VLP). Both the IPR and VLP curves relate the flowing bottom hole pressure to the surface production rate. The IPR and VLP account for what the reservoir and well can deliver, respectively. The intersection of the IPR with the VLP yields the well deliverability, which is an expression of what a well will actually produce for a given operating condition. The inception of nodal analysis came with work done by Gilbert (1954) when two-phase flow and well capabilities were analyzed by matching the inflow performance and outflow performance. This approach was named nodal analysis (Brown and Lea, 1985). The technical of nodal analysis was borrowed from the production application (production facility design) to be applied for WCD estimation. Therefore, data from reservoir

characteristics, drilling operation, and production are needed to apply nodal analysis. Typical nodal analysis, which is applied for production design considered fluid flow from the reservoir to the separator, however, nodal analysis for estimating WCD rates merely considered fluid flowing from the reservoir to the wellbore up to the wellhead (open to atmospheric pressure or subsea pressure). This is because wellbore pressure loss greatly contributes to the Vertical Lift Performance (VLP) relation in the tubing. **Figure 2.2** depicts a schematic system analysis approach that employed to estimate the WCD rate. Therefore, accurate prediction of WCD rate depends on the accuracy of the multiphase flow model employed for the analysis of flow in the wellbore. Also, to accurately analyze the flow in the wellbore, an adequate number of short wellbore segments with nodes need to be considered to ensure minimal pressure drop and approximately constant gas-liquid ratio in each segment section.

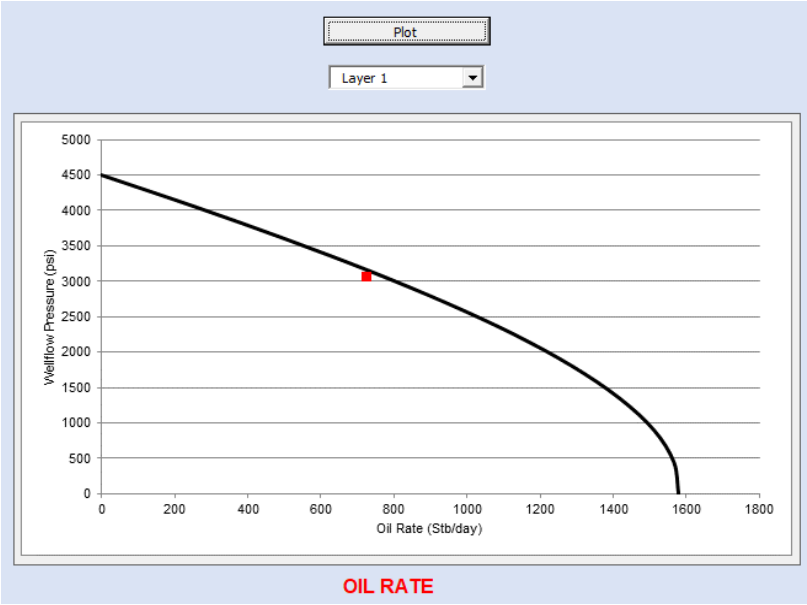

Figure 2.2 Schematic system analysis approach for estimating WCD rate

In general, there are two nodes, which are used in the program to segment the production system: 1) node No. 2 at the bottom of the hole; and 2) node No.4 at the wellhead. These are depicted in **Figure 2.3**. Since the nodal analysis in this study is applied to WCD calculation, the bottom hole node is selected to initiate the grids calculations. It is noteworthy that the calculations start from the bottom layer to the surface. Selecting the bottom hole node will divide the system into reservoir and tubing components. Since tubing component requires an iterative trial-error process, a computer program was developed to carry out pressure gradient calculation along the wellbore and optimize bottom hole pressure that is in accordance with wellhead pressure. The solution procedure of the nodal analysis for WCD calculation is listed below:

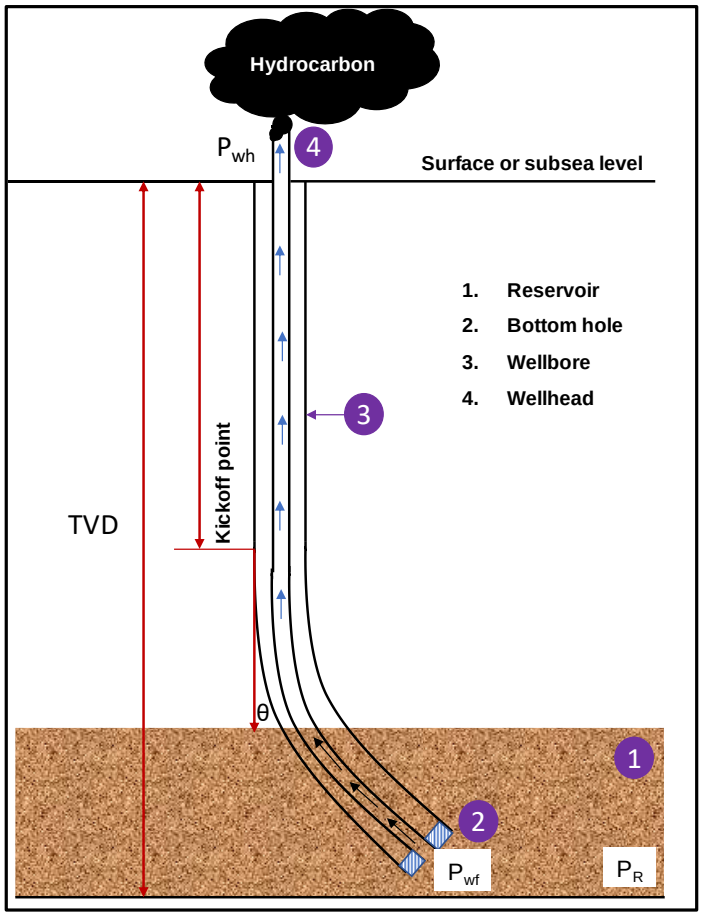

Figure 2.3 Schematic of nodal analysis for WCD scenario

1. Calculate fluid properties (density and viscosity) under reservoir conditions
2. Calculate productivity index (J) using reservoir performance model
3. Assuming bottom hole pressure (P_{wf}), the best initial guess ranges between 1 and 99% of the reservoir pressure. It is noteworthy that the calculation process starts from the bottom layer and continues upward to the wellhead.
4. Calculate liquid and gas flow rates using production models
5. Discretize the wellbore to small grids (ΔH) with the height of 1 m for each grid.
6. Once bottom hole pressure and fluid flow rates are known at point 2 in **Figure 2.3**, fluid properties (density, viscosity, oil formation factor, gas formation factor, and residual solution gas) and flow characteristics (pressure gradient, liquid hold-up) are calculated using PVT and flow models, respectively.
7. Compute differential pressure from the pressure gradient as: $\mathbf{\Delta P = \left(\frac{dp}{dH}\right)(\Delta H)}$
8. Compute pressure and temperature at the next grid point (i + 1).

$$\mathbf{P_{i+1} = P_i - \Delta P}$$

$$\mathbf{T_{i+1} = T_i - \frac{(T_B - T_S)}{H}\Delta H}$$

9. Compare local wellbore pressure with bubble point pressure. When the wellbore pressure drops below the bubble point pressure, the program accounts for the production of free gas from the liquid and updates the volumetric gas flow rate.
10. Re-calculate the fluid properties at new pressure and temperature
11. Continue Steps 7 to 9 until the next producing layer is located,
12. When a producing layer is located, the material balance equation is applied to account for additional oil and gas production.
13. Repeat steps 7 – 12 until the total number of grids is reached (wellhead)
14. Then, compare the calculated exit pressure at the last grid to the specified wellhead pressure.
15. calculated and specified pressure are matched, calculate WCD rate, gas and water rates.
16. When the exit pressure is higher than the specified wellhead pressure, then the program assumes a reduced bottom hole flowing pressure and repeat steps 2 – 14.
17. When the exit velocity is greater than sonic speed, the code increases the wellhead pressure to match two velocities.
18. In addition to the outputs mentioned in Step 15, the code generates nodal plots (IPR) **Figure 2.2**.

The required input data for WCD calculation is shown in **Table 2.1**

Table 2.1 Required input data for WCD calculation

Reservoir Data	Wellbore Data	Surface Data
Number of producing layers	Measured well depth	Wellhead pressure
Reservoir type for each layer	Kickoff point	Surface temperature
Formation type for each layer	Deviation angle from Vertical	
Reservoir pressure	Casing inner diameter	
Reservoir temperature for each layer	Open hole diameter	
Reservoir permeability for each layer	Cased hole diameter	
API gravity for each layer	Length of the open hole section	
Gas specific gravity for each layer	Hole diameter behind liner casing	
Drainage radius	Liner inner diameter	
Bubble point pressure	Casing roughness	
Gas saturation for each layer	Open hole roughness	
Water saturation for each layer	Liner roughness	
Irreducible water saturation	Casing shoe depth	
Critical gas saturation		
Critical oil saturation		
Skin factor for each layer		
Condensate yield		
Salt content		
Initial water saturation		

2.3 PVT Models

Modeling the hydrodynamic behavior of hydrocarbon in porous media and wellbore requires an accurate prediction of their PVT data. The PVT data includes all the fluid properties, which are quantity relevant to pressure and temperature such as density, viscosity, the surface tension between two-phase fluids, and formation volume factor. In addition, it is very important to identify the phase diagram of reservoir fluids.

2.3.1 PVT Properties Calculation for Gas Reservoir

Gas formation volume factor (B_g) is one of the critical parameters in the gas flow rate calculation, which is given in Eqn. (1) as a function of pressure, temperature as well as compressibility factor. (McCain, 1990)

$$B_g = 0.0282\, Z_f\, (T + 460)/P \tag{1}$$

B_g can be calculated at the reservoir or flowing bottom hole conditions, where P is a pressure (reservoir or wellbore pressure) and T is a temperature respectively. Z_f is the gas compressibility factor and it is calculated using the definition of reduced gas density (Ahmed, 2006):

$$\rho_r = \frac{0.27\, P_{pr}}{Z_f\, T_{pr}} \tag{2}$$

Dranchuk and abu-kassem (1975) proposed the following seven-constant equation of state for calculating the reduced gas density:

$$f(\rho_r) = (R_1)\rho_r - \frac{R_2}{\rho_r} + (R_3){\rho_r}^2 - (R_4){\rho_r}^5 + (R_5)\left(1 + A_{11}\,{\rho_r}^2\right)exp\left[-A_{11}\,{\rho_r}^2\right] + 1 \tag{2a}$$

With coefficients R_1 through R_5 as defined by the following relations:

$$R_1 = \left[A_1 + \frac{A_2}{T_{pr}} + \frac{A_3}{T_{pr}^3} + \frac{A_4}{T_{pr}^4} + \frac{A_5}{T_{pr}^5}\right],\ R_2 = \left[\frac{0.27\, P_{pr}}{T_{pr}}\right],\ R_3 = \left[A_6 + \frac{A_7}{T_{pr}} + \frac{A_8}{T_{pr}^2}\right],\ R_4 = A_9\left[\frac{A_7}{T_{pr}} + \frac{A_8}{T_{pr}^2}\right],\ R_5 = \left[\frac{A_{10}}{T_{pr}^3}\right]$$

The constant A_1 through A_{11} are given as following:

$A_1 = 0.3265$ $A_2 = -1.0700$ $A_3 = -0.5339$ $A_4 = 0.01569$
$A_5 = -0.05165$ $A_6 = 0.5475$ $A_7 = -0.7361$ $A_8 = 0.1844$
$A_9 = 0.1056$ $A_{10} = 0.6134$ $A_{11} = 0.7210$

where $P_{pr} = \frac{P}{P_{pc}}$ and $T_{pr} = \frac{T}{T_{pc}}$

then $P_{pc} = 677 + 15\gamma_g - 37.5\gamma_g^2$ and $T_{pc} = 168 + 325\gamma_g - 12.5\gamma_g^2$

Since gas is a compressible fluid, gas density is highly influenced by variation of pressure and temperature from the reservoir to surface conditions. Thus, it can be calculated using the following relationship and this can be expressed in kg/m^3 (McCain, 1990):

$$\rho_g = \frac{M_a P(62.40 * 1000)}{Z_f R(T + 460)} \quad (3)$$

where P is pressure (psia), T is the temperature in R°, R is gas universal constant, and M_a is an apparent molecular weight for gas, which can be obtained from Eqn. (4) as a function of gas specific gravity (McCain, 1990):

$$M_a = 29\,\gamma_g \quad (4)$$

where γ_g is gas specific gravity, which is a user input data. In fluid flow in porous media or in pipes, the gas viscosity is considered a crucial factor in calculating the gas flow rate. In this study, a correlation proposed by (Beggs and Robinson, 1975) is employed for the calculation of gas viscosity as a function of gas composition and temperature. The viscosity is given in Eqn. (5) in Pa.s (Ahmed, 2006).

$$\mu_g = A \exp\left[B\left(\frac{\rho_g}{1000}\right)^C\right] * 10^{-7} \quad (5)$$

where

$$A = \frac{9.379 + 0.01607 M_a (T^{1.5} + 460)}{209.2 + 19.26 M_a + (T + 460)}$$

$$B = 3.448 + \frac{986.4}{T + 460} + 0.01009 M_a$$

$$C = 2.447 - 0.224 * B$$

2.3.2 PVT Properties Calculation for Oil and Gas Condensate

Oil reservoir can be classified into two types, based on reservoir pressure criteria: i) under-saturated oil reservoir ($P > P_b$) and ii) saturated oil reservoir($P < P_b$). Solution gas-oil ratio is considered one of the most important characteristics of the produced oil. It remains steady when reservoir or flowing bottom pressure is above bubble point pressure. However, it gradually decreases when the pressure continuously drops below the bubble pressure. The decline in solution gas-oil ratio value occurs due to releasing of solution gas out of oil and flows as a free gas. For undersaturated oil reservoir, a correlation developed by (Elsharkawy and Alikhan, 1996) is carefully chosen to calculate solution gas-oil ratio (R_s) at bubble point pressure, which is apparently API dependent variable. For API ≤ 30, R_s can be calculated by:

$$R_s = \gamma_g P_b^{1.18026}\left[\text{antilog}_{10}\left\{-1.2179 + 0.4636\left(^{API}/_{T}\right)\right\}\right] \quad (6)$$

For API > 30, then

$$R_s = P_b^{0.94776}\gamma_g^{0.04439}\text{API}^{1.1394}[\text{antilog}_{10}\{-2.188 + 0.0008392\text{T}\}] \quad (7)$$

It is noteworthy that Eqns. (6) and (7) are valid for reservoir and production application. The typical solution gas-oil ratio trend behavior with pressure suggests that R_s remain steady (same as at bubble pressure) at a pressure higher than P_b. Therefore, the model calculated Rs at any pressure above P_b as R_{sb}. For saturated oil (P below P_b), R_s can be calculated using Eqns. (6) and (7) with replacing P_b by the actual pressure. Obviously, in Eqns. (6) and (7), Rs is given as a function of pressure, temperature, API and gas specific gravity, which known as a user input data. The oil specific gravity can be calculated by: (Ahmed, 2006).

$$\gamma_o = \frac{141.5}{(°\text{API} + 131.5)} \quad (8)$$

In this model, API is a user define input variable. In analogy to the PVT model for the gas reservoir, oil formation volume factor (B_o) is a significant variable for oil flow rate calculation. B_o is also a pressure dependent variable. The oil formation volume factor B_{ob} at bubble point pressure is expressed as (Al-Shammasi 2001):

$$B_{ob} = 1 + 5.53 * 10^{-7}[R_s(\text{T} - 60)] + 1.81 * 10^{-4}R_s\left(\frac{R_s}{\gamma_o}\right) + \frac{4.49 * 10^{-4}(\text{T} - 60)}{\gamma_o} + 2.06 * 10^{-4}\left(\frac{R_s\gamma_g}{\gamma_o}\right) \quad (9)$$

As shown in Eqn. (9), B_{ob} is directly related to the solution gas-oil ratio, temperature, gas specific gravity and inversely proportional to oil specific gravity. R_s at P <= P_b can be calculated from Eqns. (6) and (7). Additionally, Eqn. (9) can be used to predict oil formation factor for saturated oil fluid. However, for undersaturated oil condition ($P > P_b$), oil formation volume factor can be calculated by accounting for compressibility effect and using B_{ob}. It is given by (Ahmed, 2006):

$$B_o = B_{ob}\exp\left(c_o(P_b - P)\right) \quad (10)$$

where c_o denotes isothermal compressibility and given by (Farshad et al. 1996):

$$c_o = 10^{\left(-5.4531 + 5.03 * 10^{-4}\text{X} - 3.5 * 10^{-8}\text{X}^2\right)} \quad (11)$$

In Eqn. (11), X variable accounts for the influence of solution gas-oil ratio, pressure, temperature, bubble point pressure and oil specific gravity and it is given as:

$$X = R_s^{0.1982}\text{T}^{0.6685}\gamma_{\text{API}}^{-0.21435}P_b^{-0.1616} \quad (12)$$

Another important parameter that can be used to describe the flow of saturated oil is the Viscosity. For viscosity calculation, Begg-Robinson developed an empirical correlation for predicting saturated oil and gas condensate liquid viscosity. This correlation results from fitting 2073 data points. The viscosity correlation is developed based on Glaso (1980) viscosity correlation (Eqn. 16), which was proposed for calculating dead oil viscosity. The viscosity of saturated oil (cP) is given by: (Ahmed, 2006).

$$\mu_{ob} = A(\mu_{oD})^{B} \tag{13}$$

where A and B are constants, which are given by Eqns. (14) and (15), respectively.

$$A = 10.715(R_s + 100)^{-0.515} \tag{14}$$

$$B = 5.44(R_s + 150)^{-0.338} \tag{15}$$

and

$$\mu_{oD} = [3.141(10^{10})](T - 460)^{-3.444}[\log(API)]^{10.313[\log(T-460)]-36.447} \tag{16}$$

where μ_{oD} is dead oil viscosity (cP). In Eqn. (16), T is the temperature in °F. The density of gas condensate liquid is given by:

$$\rho_{gc} = \frac{62.43 \times \gamma_o}{62.43 \times 1000} \tag{17}$$

2.3.3 PVT Properties Calculation for Water Reservoir

For water production, three parameters are inquired to be calculated in order to describe the flowing behavior of water. These are water formation factor, density, and water viscosity. The water volume formation factor B_w is given by (Ahmed, 2006):

$$B_w = (A_1 + A_2)P + A_3P^2 \tag{18}$$

In Eqn. (18), A_1, A_2, and A_3 are regression model constants, which can be calculated as follows:

I. If $(P > P_b)$, the following parameters are used in calculating B_w

$$A_1 = 0.9947 + 5.8 * 10^{-6}T + 1.02 * 10^{-6}T^2$$
$$A_2 = -4.228 * 10^{-6} + 1.8376 * 10^{-8}T - 6.77 * 10^{-11}T^2$$
$$A_3 = 1.3 * 10^{-10} - 1.3855 * 10^{-12}T - 4.285 * 10^{-15}T^2$$

II. If $(P < P_b)$, these parameters are used

$$A_1 = 0.9911 + 6.35 * 10^{-5}T + 8.5 * 10^{-7}T^2$$
$$A_2 = -1.093 * 10^{-6} - 3.497 * 10^{-9}T + 4.57 * 10^{-12}T^2$$
$$A_3 = -5 * 10^{-11} + 6.429 * 10^{-13}T - 1.43 * 10^{-15}T^2$$

In the WCD model formulation, viscosity (cP) and density (kg/m^3) of water are calculated using the following correlation given by:

$$\mu_w = \exp^{(1.003 - 1.479 * 10^{-2}T + 1.982 * 10^{-5}T^2)} \quad (19)$$

and

$$\rho_w = \frac{62.368 + 0.438603Y + 1.60074 * 10^3Y^2}{62.43 * 1000} \quad (20)$$

In Eqn. (20), Y represents the salt concentration in PPM.

2.4 Production Models

This section of the report aimed to predict productivity index (PI) for oil and gas wells. Single-phase liquid exists when bottom-hole pressure is higher than bubble point pressure and at this condition; all of the gas dissolves in the liquid. Using Darcy's equation, the production can be evaluated from a well with a closed outer boundary (Brown 1984).

$$q_s = PI(P_r - P_{wf}) \quad (21)$$

where q_s flowrate (STB/d), PI is productivity index, P_r average reservoir pressure (psia), and P_{wf} is wellbore sand-face flowing pressure at the center of perforation (psia). In Eqn. (21), predicting flow rate at consistent flowing bottom hole pressure inquires known productivity index of the well. In the following section, the calculation of PI for different types of reservoirs is discussed.

2.4.1 Productivity Calculation for Gas Reservoir

If the reservoir pressure (Pr) is above 2300 psi, the gas production rate in terms of reservoir parameters in STB from (scf /d) is given by:

$$q_g = \frac{1.406 k k_{rg} h\left(\overline{P}/1000 * \overline{\mu_g}\overline{Z_f}\right)(P_r - P_{wf})}{(T_R + 460)\left[\log\left(\frac{r_e}{r_w} \div 12\right) - 0.75 + S_k\right]} \quad (22)$$

However, if P_r < 2300 psi, the gas flows rate is obtained using Eqn. (23):

$$q_g = \frac{0.703 k k_{rg} h\left(P_r^2 - P_{wf}^2\right)}{1000 \overline{\mu_g} \overline{Z_f} (T_R + 460)\left[\log\left(\frac{r_e}{r_w} \div 12\right) - 0.75 + S_k\right]} \quad (23)$$

where k and k_{rg} are absolute and relative gas permeability, h is the thickness of producing gas layer, $\overline{P}$ is an average pressure, $\overline{\mu_g}$ is average gas viscosity, $\overline{Z_f}$ is the average compressibility factor, P_r and P_{wf} are the reservoir and flowing bottom hole pressure, T_R is the reservoir temperature, r_e and r_w are reservoir and wellbore radius, and S_k is skin factor. All the average gas PVT properties in Eqns. (22 and 23) are calculated as the following:

The average gas viscosity ($\bar{\mu}_g$) is calculated through:

$$\bar{\mu}_g = \frac{\mu_{gP_r} + \mu_{gP_{wf}}}{2} \quad (24)$$

where μ_{gP_r} and $\mu_{gP_{wf}}$ are gas viscosity at the reservoir and flowing bottom hole pressure. They are calculated using the PVT gas properties model (Eqn. 5). In addition, the average gas compressibility factor ($\bar{Z}_f$) at average pressure is expressed as:

$$\bar{Z}_f = \frac{Z_{P_r} + Z_{P_{wf}}}{2} \quad (25)$$

Z_{fP_r} and $Z_{fP_{wf}}$ are compressibility factor at the reservoir and bottom hole conditions, respectively, which are also calculated from PVT gas properties model in section (2.3.1). Using Eqn. (2), $\overline{P}$ refers to the average pressure between the reservoir and wellbore, which is given by (Ahmed, 2006):

$$\overline{P} = \frac{P_r + P_{wf}}{2} \quad (26)$$

In Eqns. (22 and 23), the absolute permeability k is user input data, while gas relative permeability k_{rg} is calculated using reservoir performance model in section (2.5). As a result, Eqns. (22 and 23) provides gas production rate in scf/day (at surface condition). Thus, gas rate in rcf q_g is obtained from the following equation:

$$q_g(\text{rcf/d}) = \overline{B}_g * q_g(\text{scf/d}) \quad (27)$$

where $\overline{B}_g$ is the average gas formation volume factor which is given by:

$$\overline{B}_g = \frac{B_{gP_r} + B_{gP_{wf}}}{2} \quad (28)$$

In Eqn. (28), B_{gP_r} and $B_{gP_{wf}}$ are gas formation factor at the reservoir and flowing bottom hole pressure, respectively. They are calculated from the PVT properties gas model in section 2.3.1 using Eqn. (1). For un-condensate gas production rate $q_{g(\text{uncon})}$, the gas flow rate can be calculated by (McCain, 1990)

$$q_{g(\text{uncon})} = q_{g_{STB}} * \left[\frac{(1 - VEQ)}{R + VEQ}\right] \tag{29}$$

where VEQ and R are the volume of condensed gas and uncondensed gas, respectively. VEQ is given as follows;

$$VEQ = B_0 + B_1(P_{SP1})^{B_2}(\gamma_{SP1})^{B_3}(API)^{B_4}(T_{SP1})^{B_5}$$

where B_0 through B_5 are given by:

$B_0 = 635.530$ $B_1 = 0.361821$ $B_2 = 1.05435$

$B_3 = 5.08305$ $B_4 = 1.58124$ $B_5 = -0.791301$

Condensate production rate in STB/d is given by:

$$q_{g_{STO}} = \frac{CondY * q_{g(\text{uncon})}}{1000000} \tag{30}$$

2.4.2 Productivity Calculation for Oil Reservoir

For oil reservoir, calculation of productivity index for producing oil wells is conducted assuming three scenarios, which were classified based on the status of the reservoir and flowing bottom hole pressure. The scenarios are i) reservoir and bottom hole pressure above bubble point (P_b); ii) reservoir and bottom hole pressure below bubble point and iii) reservoir pressure above P_b and bottom hole pressure below P_b. The three cases are discussed below.

Scenario Number (I)

In this scenario, the average reservoir and flowing bottom-hole pressure are greater than the bubble point pressure ($\overline{P}_r$ and $P_{wf} > P_b$). This type of case exists in wells produced from an undersaturated reservoir. The oil flow rate is given by (Ahmed, 2006):

$$q_o = J_o(\overline{P}_r - P_{wf}) \tag{31}$$

where q_o is oil flow rate in STB/d, $\overline{P}_r$ and P_{wf} are average reservoir and bottom hole pressure, respectively, and J_o is the oil productivity index (STB/d/psi), which is calculated based on reservoir parameters and it is given by (Ahmed, 2006):

$$J_o = \frac{0.00708 k k_o h}{\bar{\mu}_o \bar{B}_o \left[\log\left(\frac{r_e}{r_w} \div 12\right) - 0.75 + S_k\right]} \quad (32)$$

where $\bar{B}_o$ and $\bar{\mu}_o$ are average oil formation factor and oil viscosity, which are calculated at average pressure and temperature using a PVT oil properties model (Eqns. 10 and 13). k and k_o are absolute and effective oil permeability, respectively. Relative oil permeability is calculated using reservoir performance model (2.5), while absolute permeability is a user input data. If there is water production accompanied with oil, then water flow rate is calculated using the following equations:

$$q_{STB/d} = J_w(P_r - P_{wf}) \quad (33)$$

where J_w is the productivity index of water and it is given by Eqn. (34):

$$J_w = \frac{0.00708 k k_w h}{\bar{\mu}_w \bar{B}_w \left[\log\left(\frac{r_e}{r_w} \div 12\right) - 0.75 + S_k\right]} \quad (34)$$

In Eqn. (34), $\bar{B}_w$ and $\bar{\mu}_w$ are average water formation volume factor and average water viscosity, which can be obtained from PVT water properties model in section 2.3.3 (Eqns. 18 and 19)? k_w is relative water permeability and is determined from the reservoir performance model. Water production rate obtained from Eqn. (33) is in STB/d. Therefore, water production rate can be estimated in bbl/d by multiplying average water formation volume factor with the water rate at a stock tank.

$$q_W = \bar{B}_w * q_{STB/d} \quad (35)$$

Scenario Number (II)

In the saturated reservoir in which the average reservoir and flowing bottom-hole pressure are below the bubble point pressure ($\bar{P}_r$ and $P_{wf} < P_b$), the oil production rate (STB/d) is given by (Ahmed, 2006):

$$q(STB/d) = J_o\left(\frac{1}{2P_b}\right)\left(P_r^2 - P_{wf}^2\right) \quad (36)$$

In Eqn. (36), oil productivity index is calculated from Eqn. (32), P_b is a bubble point pressure (psi) and it is the user input data. Similar concept, which was used for oil flow rate estimation is applied here to calculate the water production accompanied with the oil, then water flow rate (STB/d) is obtained from:

$$q_{STW} = J_w\left(\frac{1}{2P_b}\right)\left(P_r^2 - P_{wf}^2\right) \quad (37)$$

where the water productivity index is calculated using Eqn. (34). Then, water flow rate at downhole conditions is obtained using Eqn. (35). Since the reservoir and flowing bottom hole pressure are below bubble pressure, solution gas has a tendency to release out of the oil and acts as free gas. Thus, calculating free gas flowrate (scf/day) in terms of reservoir parameter is given by (Ahmed, 2006):

$$q_g = \frac{1000(kh)k_{rg}\left(P_r^2 - P_{wf}^2\right)}{1422\bar{\mu}_g\bar{Z}_f 1000(T+460)\left[log\left(\frac{r_e}{r_w} \div 12\right) - 0.75 + S_k\right]} \quad (38)$$

Then, gas flowrate in rcf/day is calculated using Eqn. (27) where gas formation volume factor is given by: (McCain, 1990).

$$B_g = 0.0282Z_f(T + 460)/P_{wf} \quad (39)$$

Scenario Number (III)

The third scenario occurs when average reservoir pressure is greater than bubble point pressure ($\bar{P}_r > P_b$) and flowing bottom-hole pressure is below the bubble point pressure($P_{wf} < P_b$). Then, the oil flow rate at STB/d is given by: (Ahmed, 2006).

$$q_o = J_o\left[\frac{1}{2P_b}\left(P_b^2 - P_{wf}^2\right) + (\bar{P}_r - P_b)\right] \quad (40)$$

Similarly, oil productivity index is obtained from Eqn. (32). $\bar{P}_r$, P_{wf} and P_b are average reservoir, flowing bottom hole and bubble pressure. While the water production rate in stock tank is given by: (Ahmed, 2006).

$$q_{STW} = J_w\left[\frac{1}{2P_b}\left(P_b^2 - P_{wf}^2\right) + (\bar{P}_r - P_b)\right] \quad (41)$$

and water flow rate in barrel/day is calculated using Eqn. (35). For gas flowrate calculation, it is given by scf/day (Ahmed, 2006):

$$q_g = \frac{1000(kh)k_{rg}\left(P_r^2 - P_{wf}^2\right)}{1422\bar{\mu}_g\bar{Z}_f 1000(T+460)\left[log\left(\frac{r_e}{r_w} \div 12\right) - 0.75 + S_k\right]} \quad (42)$$

Then, the gas rate is calculated in rcf/day using Eqn. (27) in which gas formation volume factor is obtained from Eqn. (28).

2.5 Reservoir Performance Model

Reservoir performance model is estimated by the following equations.

2.5.1 Relative Permeability

To estimate the productivity index for oil or gas well, reservoir characteristics such as absolute and relative permeability, reservoir thickness, and reservoir fluid saturation are essential. For undersaturated reservoir($P_r \geq P_b$), oil saturation is calculated by (Ahmed, 2006):

$$S_o = 1 - S_g - S_w \tag{43}$$

However, the effective oil saturation (S_o^*) is given by Eqn. (44):

$$S_o^* = \frac{S_o}{1-S_w} \tag{44}$$

For unconsolidated reservoir type, the relative permeability of water, oil and gas fluid in a water-wet system is calculated as following (Ahmed, 2006):

If ($S_w \geq S_{wc}$), the relative permeability of water (k_{rw}) is given by:

$$k_{rw} = \left(\frac{S_w - S_{wc}}{1-S_{wi}}\right)^3 \tag{45}$$

where S_{wi} is irreducible water saturation, S_w denotes water saturation and S_{wc} critical water saturation. If ($S_o \geq S_{oc}$), the oil relative permeability (k_{ro}) is given by (Ahmed, 2006):

$$k_{ro} = \frac{(S_o)^3}{(1 - S_{wc})^3} \tag{46}$$

where S_{oc} is critical oil saturation and S_o symbolizes oil saturation. The relative permeability for gas (k_{rg}) is:

$$k_{rg} = \frac{(S_o)^3(2S_w + S_o - 2S_{wc})^4}{(1 - S_{wi})^4} \tag{47}$$

If ($S_g \geq S_{gc}$), where S_g is gas saturation while S_{gc} represents critical gas saturation, the relative permeability of gas in a gas – oil system was determined using an expression proposed by Torcaso and Wyllie (1958) as following (Ahmed, 2006):

$$k_{rg} = k_{ro}\left[\frac{(S_o^*)^4}{(1 - S_o^*)^2\,(1 - (S_o^*)^2)}\right] \tag{48}$$

The following was employed to determine the relative permeability of another type of reservoir. If ($S_w \geq S_{wc}$), the relative permeability of water is given by (Ahmed, 2006)

$$k_{rw} = \left(\frac{S_w - S_{wc}}{1 - S_{wc}}\right)^4 \quad (49)$$

If $(S_o \geq S_{oc})$, the relative permeability of oil is given by (Ahmed, 2006):

$$k_{ro} = \frac{S_o^3(2S_w + S_o - 2S_{wc})}{(1 - S_{wc})^4} \quad (50)$$

If $\left(S_g \geq S_{gc}\right)$, the relative permeability of gas in oil using Torcaso and Wyllie correlation is given by (Ahmed, 2006):

$$k_{rg} = k_{ro}\left[\frac{(S_o^*)^4}{(1 - S_o^*)^2\,(1 - (S_o^*)^2)}\right] \quad (51)$$

Experimental data from Li and Horne (2006) is employed to develop correlations for relative permeability of gas and water (k_{rg} and k_{rw}). The relative permeability for gas is expressed as:

$$k_{rg} = -0.8536S_w^3 + 3.4657S_w^2 - 4.3498S_W + 1.7386 \quad (52)$$

and water relative permeability is given by:

$$k_{rw} = 1.2156S_w^3 + 0.0638S_w^2 - 0.3167S_W + 0.0531 \quad (53)$$

2.5.2 Interfacial Tension

The interfacial tension σ can be defined as the exerted force that exists between the boundary layer of the liquid phase and vapor or gas phase per unit length. This can be expressed as follows

$$\sigma = \frac{\left[P_S\left(\frac{\rho_L}{1000} - \frac{\rho_g}{1000}\right)\frac{M}{4}\right]}{1000} \quad (54)$$

2.6 Fluid Flow Behavior in the Wellbore

In the petroleum industry, gas-liquid two-phase flow occurs inside wellbores, risers, and pipelines, during production operation and blowout incidents. Due to a dramatic change in pressure along the wellbore, different flow patterns can possibly develop at different depths. For instance, near the bottom of the wellbore, we may have only one phase. As the fluid moves upward, its pressure

gradually decreases. At the point where the pressure drops below the bubble point pressure, dissolved gas will start releasing out of the liquid and the flow pattern will be bubbly. As pressure decreases further, more gas may come out of solution and we may see the whole range of flow patterns, as shown in **Fig. 2.4**. An accurate prediction of pressure drop along the wellbore inquires a precise identification of flow patterns. Therefore, an extensive study was conducted to investigate the hydrodynamic conditions that give rise to the various flow-pattern transitions.

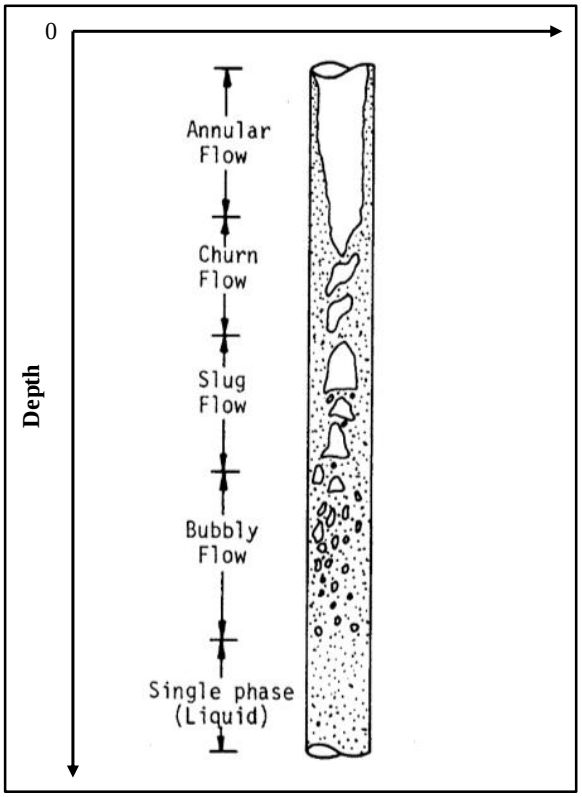

Figure 2.4 Schematic of expected two-phase flow pattern in the wellbore (Modified after Hasan and Kabir 1988)

Prior to developing WCD computational tool, an extensive literature survey was carried out reviewing experimental and modeling studies at various flow conditions to determine total pressure behavior with superficial gas and liquid velocities. Total pressure gradient in the wellbore consists of three components including gravitational (hydrostatic), friction and acceleration, as given by the following equation:

$$\left(\frac{dp}{dl}\right)_T = \left(\frac{dp}{dL}\right)_g + \left(\frac{dp}{dL}\right)_f + \left(\frac{dp}{dL}\right)_A \tag{55}$$

In most two-phase flow studies in vertical or horizontal pipes, the third component has a small influence on total pressure drop, particularly at low superficial gas velocity. Therefore, it was neglected in the existing modeling development. **Figure 2.5** presents a schematic of the total pressure gradient behavior for vertical flow (Shoham, 2005). **Figure 2.5** was developed for a constant superficial liquid velocity. However, total pressure gradient constantly increases with superficial liquid velocity. As displayed in the figure, the total pressure gradient in the wellbore declines with an increase in the superficial gas velocity. This is due to the reduction in the gravitational component. This reduction occurs mainly because of the lower liquid holdup in the system. The decline in pressure gradient progressively continues until it reaches a critical point at which gravitational and friction components are balanced. Afterward, a further increase in superficial gas velocity results in a sharp elevation of the total pressure gradient. This increment is attributed to the high flow resistance (frictional pressure gradient). Thus, the total pressure gradient, which is the sum of the gravitational and frictional pressure gradient components, exhibits a minimum value at the critical point, usually occurring under slug flow conditions. Based on our comprehensive theoretical study and validation of different mechanistic two-phase

models, we have segregated the total pressure gradient trend to four regions: low superficial gas velocity region; transient region; high superficial gas velocity region and extremely high velocity (sonic and supersonic velocity) region.

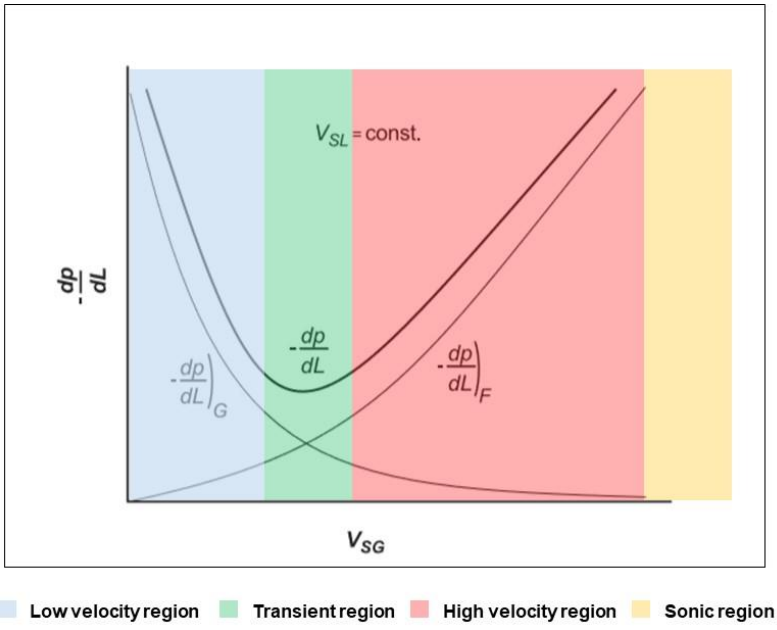

Fig. 2.5 Schematic of pressure gradient behavior in vertical flow (Modified after Shoham, 2005)

In the oil and gas field operations, there is no such thing as a truly vertical borehole; however, wells that aim at a target directly below its surface location are considered vertical wells. In oil field development, directional drilling may be considered as the best option for several reasons such as sidetracking, controlling vertical wells, drilling beneath inaccessible locations, and relief well etc. With respect to the wellbore hydrodynamic, inclination angle has a significant effect on total pressure gradient, partiality at low superficial gas velocity region in which gravitational component is dominated. In addition, flow patterns of two-phase fluids moving upward in the vertical pipe is different from those might be developed in the horizontal pipe. However, Hernandez Perez, 2008 reported that flow patterns observed in upward inclined flow are relatively analogous to those observed in vertical upward flow, particularly for near-vertical systems. **Figure 2.6** shows flow patterns that can be developed in both vertical and inclined pipe. These patterns include bubbly and dispersed bubbly, slug, churn and annular flow. For systems deviated more than 20° from vertical, churn flow is rarely observed. Hernandez Perez (2008) carried out an experimental study to investigate gas-liquid two-phase flow in inclined pipes. The experiments were carried out at low superficial gas velocity range (0.17 – 3.35 m/s). During the test, the inclination angle was varied from -5 (downward flow) to 90° from the horizontal level. The test measurement of the pressure gradient with superficial gas velocity is presented in **Figure 2.7a**. After analyzing Perez's data, it is found that slight deviation from the vertical (up to 30°) has an insignificant effect on the pressure gradient measurement. However, the pressure gradient

was considerably reduced as the inclination angle increased up to 60° from the vertical position. A similar observation was obtained at high superficial gas velocity measurement (Luo et al. 2016), as shown in **Figure 2.7b**.

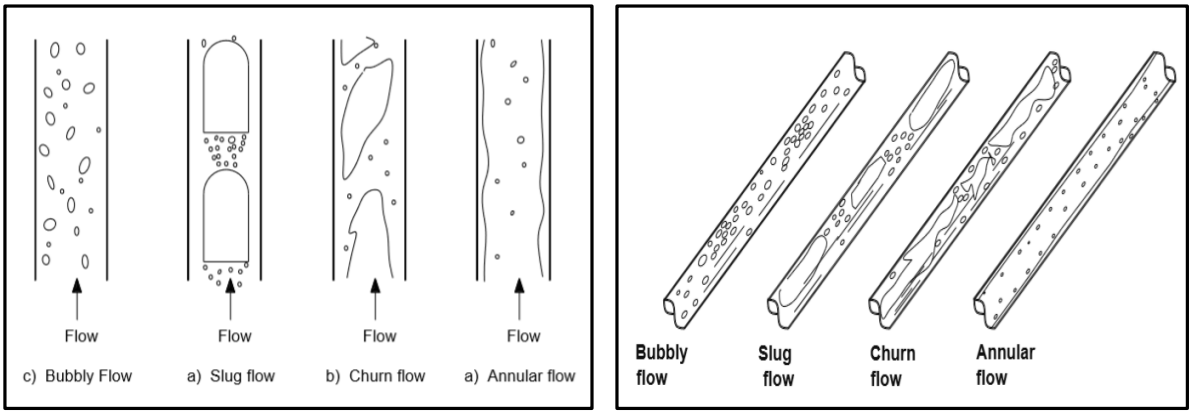

Figure 2.6 Flow patterns of gas/liquid flow in pipes: a) Vertical and b) inclined (Hernandez Perez, 2008)

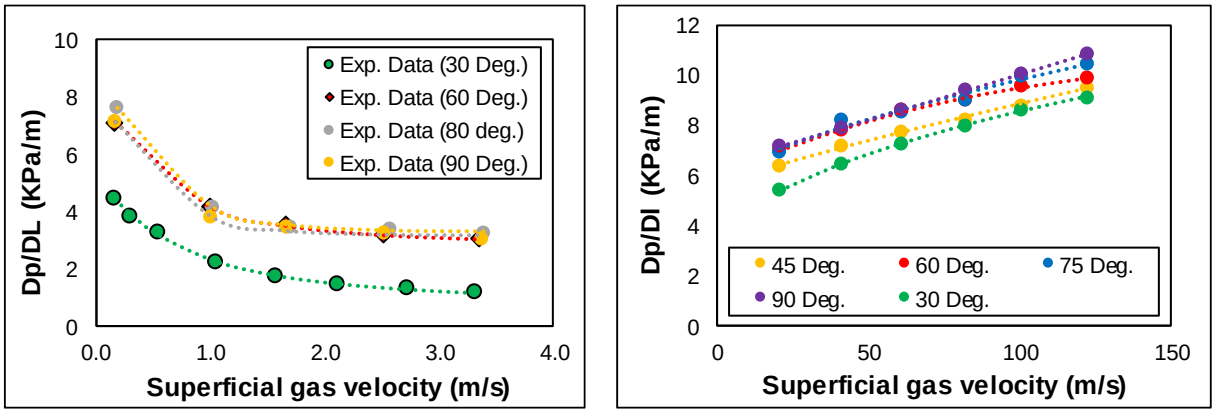

(a) **(b)**

Figure 2.7 Effect inclination angle on the pressure gradient at a) low superficial gas velocity (Hernandez Perez, 2008) and b) high superficial gas velocity (Luo et al. 2016)

2.7 Modeling Single-phase Flow Characteristics in Pipe

As pointed out in section 2.6, there is a possibility for the flow to be a single phase at the bottom of the wellbore. The single phase can be pure gas or liquid fluid. Since the pressure drop calculation along the wellbore is a proportional and sequential process, an accurate prediction of pressure at first step is a very crucial factor. Pressure loss for single flow consists of gravitational and friction component and is a proposition to fluid properties, fluid velocity, pipe size, and roughness as well as inclination angle. The total pressure gradient in the pipe is given by the following equation:

$$\left(\frac{\mathrm{dp}}{\mathrm{dL}}\right)_{\mathrm{T}} = \rho_F g \sin\theta + \frac{2 f_f \rho_F V_F^2}{\mathrm{D}} \qquad (56)$$

where $\left(\frac{\mathrm{dp}}{\mathrm{dL}}\right)_{\mathrm{T}}$ is total pressure gradient (Pa/m), f_f is a fanning friction factor, θ is the inclination angle of the test section measured from the horizontal (degree), g is gravity acceleration (m/s^2), D is the hydraulic diameter of the test section, ρ_F is fluid density, and V_F is fluid velocity. The friction factor used in the calculation of predicted pressure loss is shown in Equation (57). This was developed by Chen (1979).

$$\frac{1}{\sqrt{f_D}} = -2.0\ log\left[\frac{\varepsilon}{3.7065D} - log\left(\frac{1}{2.8257}\left(\frac{\varepsilon}{D}\right)^{1.1098} + \frac{5.8506}{N_{Re}^{0.8981}}\right)\right] \quad (57)$$

where f_D is Darcy friction factor, which is defined as fourfold Fanning friction factor, ε is the pipe roughness, N_{Re} is a Reynold number. The model predictions of pressure loss for a single-phase (water) flow into vertical pipe were validated with experimental data, which was obtained using OU – Lab test setup. The comparison between measured and predicted pressure drop is shown in Section (2.9).

2.8 Modeling Two-phase Flow Characteristics in Pipe

Two-phase flow occurs in the petroleum industry during oil and gas production and transportation. The flow of oil and gas occur in horizontal, inclined, or vertical pipes, in both the wellbore and the flowline. In offshore production, flowlines carrying oil and gas can be far from the process facilities. Components, such as pipes, separators, or slug catchers are used for the flow control and process.

Multiphase flow characteristics such as the velocity of phases, flow patterns, and geometry will influence WCD. Multiphase flow is a common occurrence in oil and gas operations. This fluid dynamics problem leads to the question of understanding the mechanisms behind the multiphase flow system. The efforts to understand and characterize the intricacies of flow started with the development of empirical correlations and with time-shifted towards mathematical modeling and simulation approach. Statistical analysis and interpretation of experimental results are used to develop empirical correlation and mechanistic models. The mechanistic approach is developed based on the understanding of the mechanism of the combined momentum balance equations for each phase**.**

2.8.1 Flow Patterns Map for Vertical Pipe

Different flow configuration or flow patterns exist when gas and liquid flow simultaneously in a pipe and distribute themselves into phases. Flow patterns depend on operational conditions, geometric variables and physical properties of the phases. The following flow patterns exist in the vertical pipe: bubbly, dispersed bubble, slug, churn and annular flow and their transition. In **Figure 2.8**, the flow pattern that occurs in the vertical conduit is shown with the boundary, which is the transition of one flow regime to the other (Tengesdal et al., 1999).

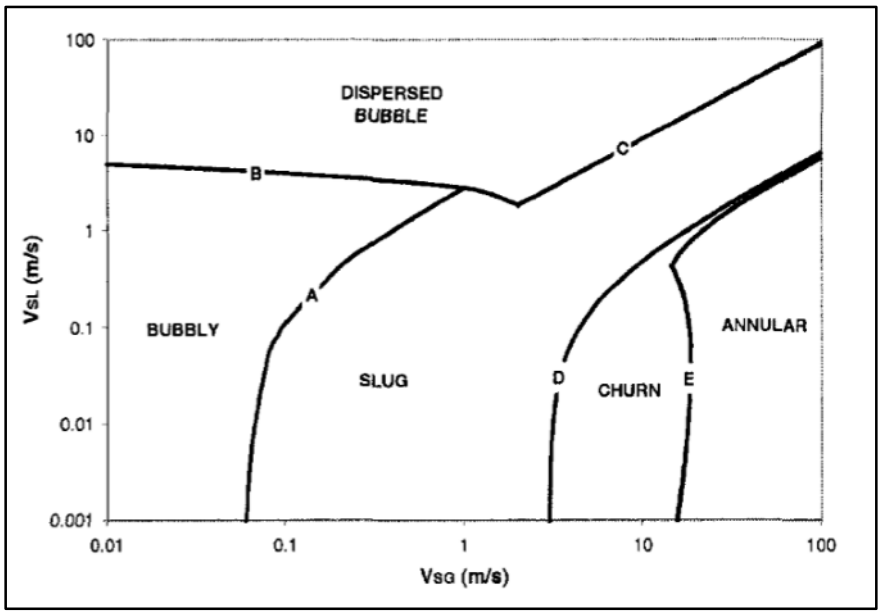

Figure 2.8 Flow pattern map (Tengesdal et al., 1999)

Bubble flow exists at low gas velocity and low to moderate liquid velocity. In this flow pattern, bubbles move faster than the liquid phase due to slippage. However, in dispersed bubble flows the two phases flow at the same velocity (as the liquid velocity increases). This leads to non-slip flow conditions. The increase of gas flow rate changes the pattern of the flow to slug which is characterized by bullet-shaped bubbles formed as a result of the coalesce of dispersed bubbles and follows by liquid slug body, which bridges the entire cross-sectional area of the pipe and contains small spherical distributed gas bubbles. The bullet-shaped bubbles are called Taylor bubbles. Churn flow occurs at the higher gas flow and causes Taylors bubbles to break down thereby destroying the bridging across liquid slugs. The subsequent gas movement sweeps the liquid upward thereby resulting in the oscillatory liquid flow. At high gas velocity, the liquid flows on the wall of the pipe and the gas phase with small liquid droplet flows in the center, this flow regime is called annular. The transition of flow exists between various flow patterns. Bubble flow can transit to disperse bubble or low-velocity slug depending on the operating conditions. In addition, the slug can be transmitted to churn at high velocity and annular flow can transit to mist or slug at high velocity. The derivation of equations that describe the transition between various flows patterns in the vertical pipe is widely discussed elsewhere (Tengesdal et al., 1999; Ansari et al. 1994; Hasan and Kabir 1988). However, the final equations that define boundaries between different flows patterns as shown in **Figure 2.8** are summarized in **Table 2.2**.

Table 2.2 Summary of flow pattern identification boundary.

Reference	Flow pattern transition	Boundary	Equation
Tengesdal et al. (1999)	Bubble - Slug	A	$V_{Sg} = 0.37V_{Sl} + 0.48[g\sigma_L(\rho_L - \rho_G)/\rho_L^2]^{0.25}$
Wu et al. (2017)	Bubble - Dispersed Bubble	B	$V_{Sl} = 6.14D^{0.43}\left(\frac{\sigma_L}{\rho_L}\right)^{0.54}\left(\frac{\rho_L}{\mu_L}\right)^{0.071}(g(\rho_L - \rho_G)/\sigma_L)^{0.45} - V_{Sg}$
Tengesdal et al. (1999)	Slug - Dispersed Bubble	C	$V_{Sl} = 0.93V_{Sg}$
Tengesdal et al. (1999)	Slug - Churn	D	$V_{Sg} = 12.19\left(1.2V_{Sl} + 0.35\left[gD\left(\rho_L - \rho_g\right)/\rho_L\right]^{0.5}\right)$
Ansari et al. (1994)	Slug - Annular	E	$V_{Sg} = 3.1[g\sigma_L(\rho_L - \rho_G)/\rho_G^2]^{0.25}$

The modified flow pattern map for WCD tool is shown in **Figure 2.9.** This is developed based on an intensive study of different mechanistic models available in the literature. This map assists in defining the applicability limits of each model that is integrated inside the WCD tool based on both superficial gas and liquid velocities. As displayed from the figure, the fluid flow models incorporated in the WCD tool consists of various mechanistic models including bubble and dispersed bubble flow model, low-velocity slug model, annular flow model, and high-velocity slug flow model. It is noteworthy that high-velocity slug flow pattern has not been observed in any of the existing experimental studies. However, this flow pattern was observed from OU-lab data at extremely high liquid velocity. The accuracy of the modified flow pattern map for WCD tool was tested and validated with the data acquired from the experiments. For high flow conditions in a vertical pipe, data from the experiments carried out in Well Construction and Technology Centre of the Department of Petroleum Engineering were employed to validate high flow rate conditions. On the other hand, the validation of low flowrate two-phase conditions in the vertical pipe was carried out using data from other investigators. In **Figure 2.9,** considering liquid superficial velocity between 0 to 1.5 m/s and above, increasing the superficial gas velocity will result in different flow patterns shown in **Figure 2.9**.

The hybrid flow patterns in **Figure 2.9** are complex flow patterns that occurred because of an enormous jump in the pressure gradient from one-flow patterns to the other. The hybrid predicts with two different models. One of the two models predict at the maximum while the other model at the minimum.

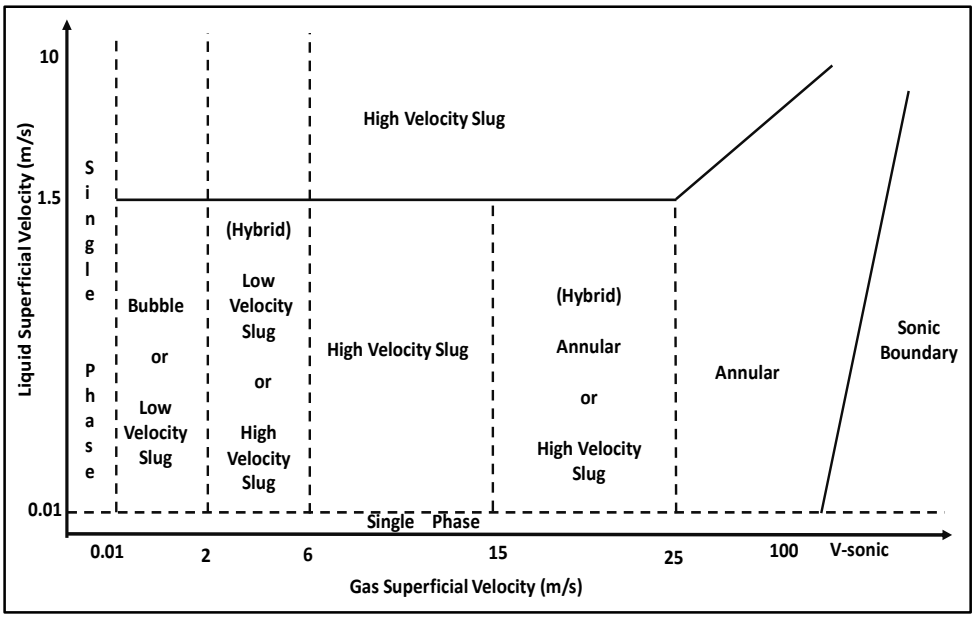

Figure 2.9 Modified flow pattern map for WCD – computational tool

According to modified flow map (Figure 2.9), at extremely low superficial gas velocity (Vsg < 0.01 m/s), the flow is considered single liquid phase. At superficial gas velocity range of 0.01 and 2 m/s, the flow can be bubble or slug flow. The condition which small bubbles from bubbly flow agglomerate and becomes Taylor bubble is the transition of bubbly flow to slug flow. Experimentally this transition occurs at a void fraction between 0.25 and 0.3 (Griffith and Snyder, 1964). The transition between bubbly flow and low-velocity slug flow is governed by the critical value of superficial gas velocity, which is defined in **Table 2.2**.

2.8.2 Pressure Gradient Prediction in Vertical and Near Vertical Pipe

Once the flow pattern of the two-phase flow is accurately predicted, subsequently, the total pressure gradient can be calculated using the most suitable mechanistic model. In this section, the formulation of various two-phase flow models and flowchart that describes the calculation process of each model is presented. It is noteworthy that these models can provide satisfactory predictions of the pressure gradient in the inclined wellbore up to 45°.

2.8.2.1 Bubbly Flow

For predicting the pressure gradient in the bubble flow regime, a model developed by Hasan and Kabir (1988) was adopted. As well known that total pressure gradient at low superficial gas velocity can be calculated using the following equation:

$$\left(\frac{dp}{dL}\right)_T = \left(\frac{dp}{dL}\right)_e + \left(\frac{dp}{dL}\right)_f \tag{58}$$

The initial step in the pressure gradient calculation is that predicting the void fraction at given superficial gas and liquid velocities. By applying the drift flux model and in-site gas velocity

concept, Hasan and Kabir (1988) developed a form to calculate the void fraction α for bubbly flow using Eqn. (59):

$$\alpha = \frac{v_{Sg}}{C_0 v_m + v_\infty} \tag{59}$$

where C_0 is bubbly flow variable, which is proportional to pipe size and superficial liquid velocity $C_0 = 1.2$ if $d < 0.12$ m or if $v_{SL} > 0.02$ m/s and $C_0 = 2$ if $d > 0.12$ m or $v_{SL} < 0.02$ m/s. v_∞ is the terminal rise-velocity of the bubble and it is given by:

$$v_\infty = 1.53\left[g\sigma_L\left(\rho_L - \rho_g\right)/\rho_L{}^2\right]^{0.25} \tag{60}$$

Then, the density of the bubbly fluid (mixture density), ρ_m is calculated proportional to liquid and gas densities as well as void fraction, which is expressed as:

$$\rho_m = \rho_g \alpha + \rho_L(1 - \alpha) \tag{61}$$

In Eqn. (62), the elevation or gravitational component of the total pressure gradient is given by

$$\left(\frac{dp}{dL}\right)_e = \rho_m g Sin\theta \tag{62}$$

where θ is the inclination angle of the wellbore that is measured from the horizontal level. In Eqn. (63), the friction component of the total pressure gradient, which is considered less dominated factor at low superficial gas velocity, can be given by:

$$\left(\frac{dp}{dL}\right)_f = \frac{f_D \rho_m v_m^2}{2d} \tag{63}$$

where v_m is mixture velocity, which is defined as a summation of superficial gas and liquid velocities (m/s), d is pipe diameter (m), and f_D is a Darcy friction factor that can be estimated from the Moody diagram or using the following equation:

$$\frac{1}{\sqrt{f_D}} = -1.8log\left[\frac{6.9}{N_{Re}} + \left(\frac{\varepsilon/d}{3.7}\right)^{1.11}\right] \tag{64}$$

where ε is an absolute pipe roughness, and N_{Re} is the Reynolds number of the bubbly flow, which can be calculated using Eqn. (65).

$$N_{Re} = \frac{\rho_m v_m d}{\mu_m} \tag{65}$$

In Eqn. (66), μ_m is a mixture dynamic viscosity of the bubbly fluid and it is related proportional to both gas and liquid viscosity as well as the gas fraction in continuous liquid phase, which can be expressed as following:

$$\mu_m = \mu_g \alpha + \mu_L (1 - \alpha) \tag{66}$$

2.8.2.2 Low-Velocity Slug Model

As superficial gas velocity increases, the flow pattern of two-phase fluid may change from being bubbly to slug flow. The principle of this transition is a coalescence of the small gas bubble into large Taylor bubble (Hasan and Kabir 1988; Ansari et al. 1994). Experimentally, it was found that bubble-slug transition occurs at 0.25 of void fraction. This finding was translated to equation (Table 2.2) in terms of superficial gas and liquid velocities, which is considered as transition criteria. An analogy technique (combination of drift flux model and in-situ gas velocity), which was applied to bubble flow model is used by Hasan and Kabir (1988) to calculate the void fraction for slug flow pattern at low superficial gas velocity:

$$\alpha = \frac{v_{Sg}}{\left[1.2 v_m + 0.345 \left(\frac{g \sigma_L (\rho_L - \rho_g)}{\rho_L}\right)^{0.5}\right]} \tag{67}$$

Once the void fraction is obtained, density and viscosity of slug flow are calculated using Eqns. (61) and (66), respectively. Subsequently, the pressure gradients due to gravitational and friction effect are calculated using Eqns. (62) and (63). Eventually, the total pressure gradient is obtained from the summation of two components. In this study, a simple algorithm is developed to describe the calculation procedure of the pressure gradient for bubbly and slug flow, as presented in **Figure 2.10**.

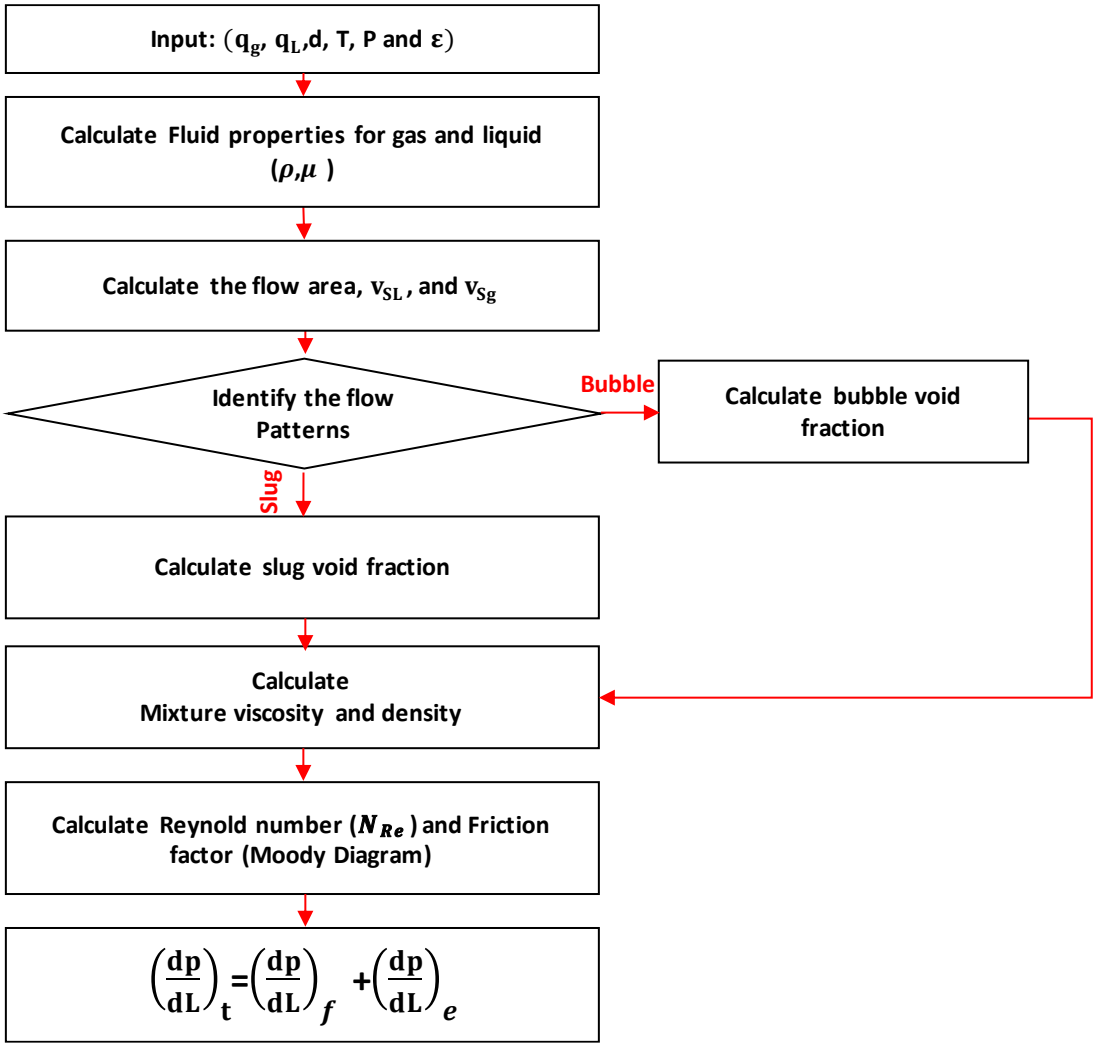

Figure 2.10 Flow chart for bubble and low-velocity slug flow

2.8.2.3 High-Velocity Slug Model

Slug flow is a common flow pattern-taking place in the wellbore. It has a configuration of a series of Taylor bubbles segregated by liquid slugs. Various mechanistic models were developed to simulate the slug flow in the pipe. However, none of these models was tested at high liquid and gas flow rate conditions. A schematic of a developed slug unit is shown in **Figure 2.11**. A full description of the model formulation is presented in the following section.

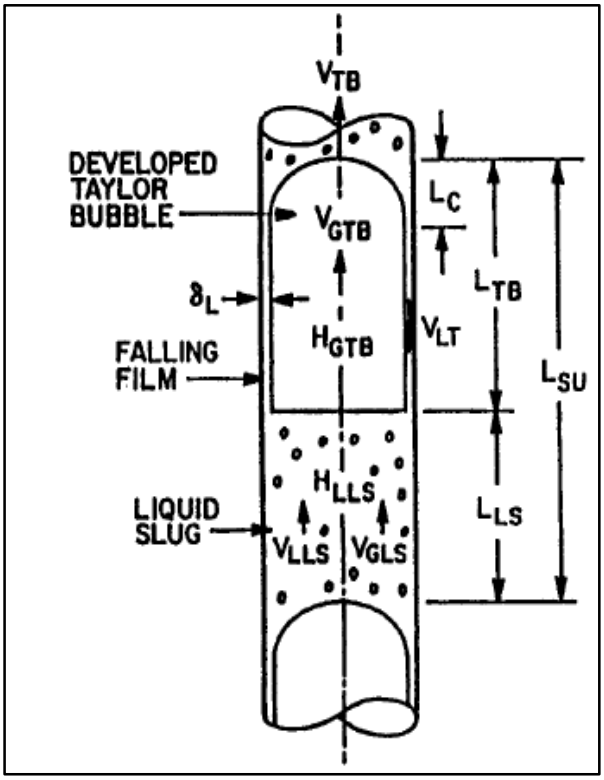

Figure 2.11 Schematic slug units for developed slug unit (Ansari et al. 1994)

For fully developed slug unit, the overall gas and liquid mass balances give:

$$v_{Sg} = \beta v_{gTB}(1 - H_{LTB}) + (1 - \beta)v_{gLS}(1 - H_{LLS}) \tag{68}$$

and

$$v_{SL} = (1 - \beta)v_{LLS}H_{LLS} - \beta V_{LTB}H_{LTB} \tag{69}$$

where β is defined as:

$$\beta = {}^{L_{TB}}/_{L_{SU}} \tag{70}$$

Mass balances for gas and liquid from the liquid slug to Taylor bubble give the following equations:

$$(v_{TB} - v_{LSS})H_{LLS} = \left[v_{TB^{-(-V_{LTB})}}\right]H_{LTB} \tag{71}$$

and

$$\left(v_{TB} - v_{gLS}\right)(1 - H_{LLS}) = \left(v_{TB^{-v_{gTB}}}\right)(1 - H_{LTB}) \tag{72}$$

The Taylor bubble- rise velocity is equal to the summation of centerline velocity and Taylor bubble-rise velocity in stagnant liquid column

$$v_{TB} = 1.2v_m + 0.35\left[\frac{gd(\rho_L - \rho_g)}{\rho_L}\right]^{0.5} \tag{73}$$

By applying a similar concept, the velocity of the gas bubbles in the liquid slug is:

$$v_{gLS} = 1.2v_m + 1.53\left[\frac{gd(\rho_L - \rho_g)}{\rho_L^2}\right]^{0.25} H_{LSS}^{0.5} \tag{74}$$

where the second term in Eqn. (74) represents the bubble-rise velocity. As the slug unit is moving upward, the liquid film surrounding Taylor bubble will be moving downward. Falling film velocity can be correlated with film thickness with the Brotz (1954) expression:

$$v_{LTB} = (196.7g\delta_L)^{0.5} \tag{75}$$

where δ_L denotes film thickness for developed slug flow and it can be expressed in terms of Taylor bubble void fraction. As a result, the falling film velocity can be rewritten as:

$$v_{LTB} = 9.916\left[gd\left(1 - \sqrt{H_{gTB}}\right)\right]^{0.5} \tag{76}$$

The equation scheme consisting of seven equations, (68) or (69), (70) (overall gas and liquid mass balances and mass balances for liquid and Taylor bubble) through (74), then (76) contains eight unknowns variables that define the slug flow model including β, H_{gLS}, H_{LTB}, v_{LTB}, v_{gTB}, v_{gLS}, v_{LLS}, and v_{TB}. In order to close the model, one additional equation is needed. Based on experimental data developed by Fermandes et al. (1986) and Schmidt (1976), Sylvester (1987) proposed a correlation for predicting the liquid slug void fraction as a function of superficial gas velocity and mixture velocity, which is expressed as:

$$H_{gLS} = \frac{v_{Sg}}{0.425 + 2.65v_m} \tag{77}$$

By integrating Eqn. (77), a non-linear system consisting of eight equations and eight unknowns is established. An iterative process is needed to solve these unknowns. For simplicity, Vo and Shoham (1989) indicated that combining these eight equations algebraically will result in equation (78).

$$\left(9.916\sqrt{gd}\right)\left(1 - \sqrt{1 - H_{LTB}}\right)^{0.5} H_{LTB} - v_{TB}(1 - H_{LTB}) + \overline{A} = 0 \tag{78}$$

where

$$\overline{A} = H_{gLS} v_{TB} + (1 - H_{gLS}) * \left[v_m - H_{gLS} \left\{ 1.53 \left[\frac{\sigma_{Lg}(\rho_L - \rho_g)}{\rho_L^2} \right]^{0.25} (1 - H_{gLS})^{0.5} \right\} \right] \quad (79)$$

Eqn. (78) is numerically solved for H_{LTB} using the Bisection method. Once the value of average liquid holdup in Taylor bubble is determined, then the other slug flow variables can be determined. A simple schematic shown in **Figure 2.12** is developed to summarize step-by-step procedures that are used to determine all slug variables.

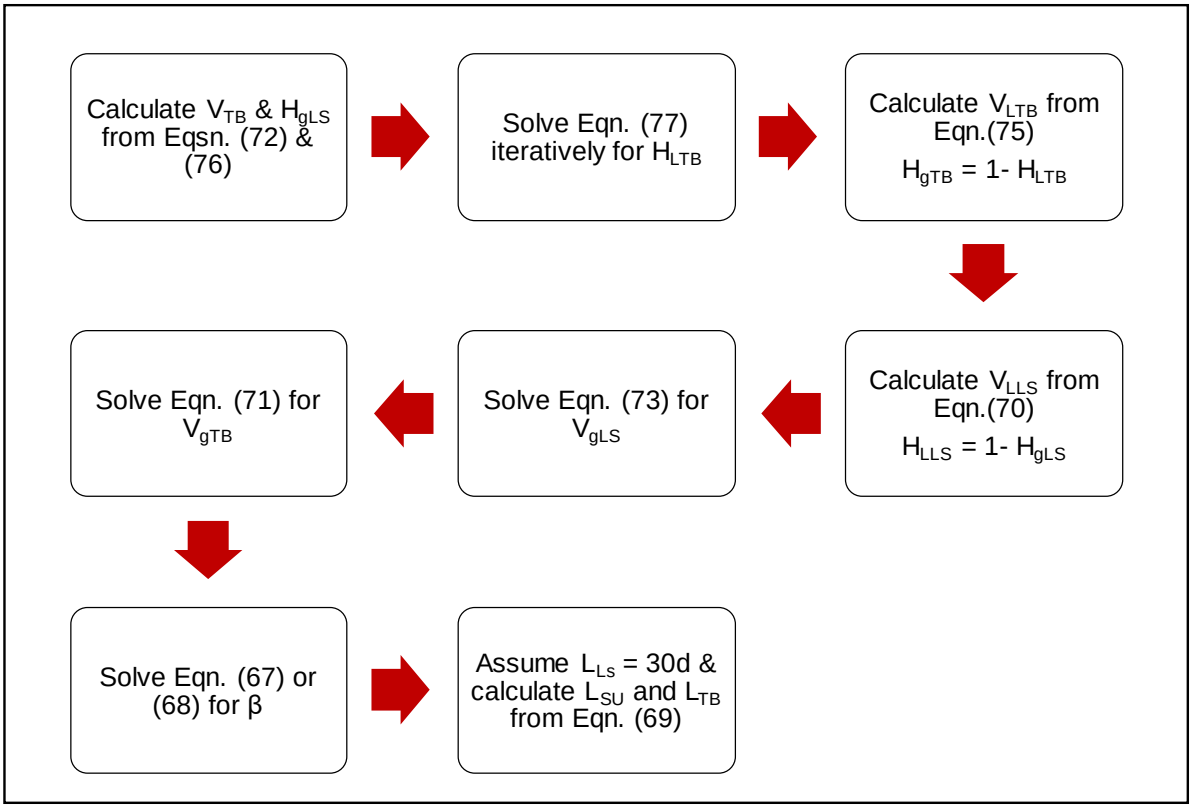

Figure 2.12 Schematic for calculation procedure of slug flow variables

In calculating pressure gradients (gravitational and frictional components), Ansari et al. accounted for the influential role of varying film thickness and neglected the friction contribution along the Taylor bubble. In this case, the total pressure is calculated using Eqn. (56), in which the elevation or gravity component across the slug unit for developed flow is given by:

$$\left(\frac{dp}{dL}\right)_e = [(1 - \beta)\rho_{LS} + \beta\rho_g] g sin\theta \quad (80)$$

where

$$\rho_{LS} = \rho_L H_{LLS} + \rho_g (1 - H_{LLS}) \quad (81)$$

Also, in Eqn. (58), the friction component of the total pressure gradient is expressed as follows:

$$\left(\frac{dp}{dL}\right)_f = \frac{f_{LS}\,\rho_{LS} v_m^2}{2d}(1-\beta) \tag{82}$$

where f_{LS} is the friction factor of liquid slug and it can be obtained from the Moody diagram or Eqn. (64) as a function of Reynolds number (N_{ReLS}), which is given as:

$$N_{ReLS} = \frac{\rho_{LS} v_m d}{\mu_{LS}} \tag{83}$$

The algorithm that describes the calculation procedure of pressure gradient for high velocity slug flow is presented in **Figure 2.13**.

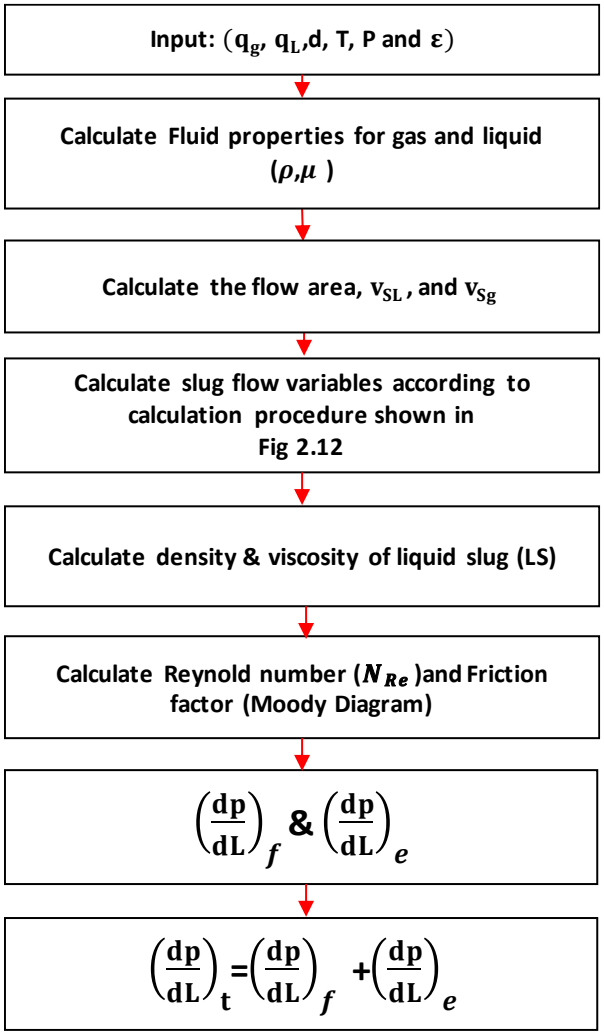

Figure 2.13 Flow chart for high-velocity slug model

2.8.2.4 Annular Flow Model

Annular flow pattern develops when gas and liquid flow concurrently upward at high superficial gas velocity and relatively low liquid rate. The annular flow is characterized by a liquid film

surrounding a gas core. The schematic of a fully developed annular flow pattern in the pipe is depicted in **Figure 2.14**. As displayed in the figure, the gas flows in the core, while liquid flows both in the core, as entrained droplets, and film at the wall of the pipe. Various mechanistic models (Ansari et al. 1994; Hasan and Kabir 1988; Tengesdal et al. 1999) were developed to simulate annular flow in the pipe. None of these models was tested at high flow conditions. Therefore, these models were validated with OU – Lab data under a wide range of superficial gas and liquid velocities, as a result, Ansari et al.'s mechanistic model was selected and modified as the best option to simulate high flow rate conditions. In the following section, a detailed annular flow model and calculation procedure is presented.

For a fully developed annular flow with a stable liquid film, applying conservation of momentum separately to the core and the film yields:

$$A_c \left(\frac{dp}{dL}\right)_c - \tau_i S_i - \rho_c A_c g sin\theta = 0 \tag{84}$$

and

$$A_F \left(\frac{dp}{dL}\right)_F + \tau_i S_i - \tau_F S_F - \rho_L A_F g sin\theta = 0 \tag{85}$$

where $\left(\frac{dp}{dL}\right)_c$ and $\left(\frac{dp}{dL}\right)_F$ are pressure gradient at gas core and liquid film for the pipe segment, respectively. In this model, it is assumed that pressure gradient is merely varied in the axial direction and steady in the radial direction. Therefore, both values are equal and equivalent to the total pressure gradient, A_c and A_F are gas core and liquid film area, respectively, τ_i and τ_F are interfacial and film shear stress, S_i and S_F represent interfacial and liquid film wetted perimeter, ρ_c and ρ_L denote core and liquid densities, and θ is the inclination angle from the horizontal level (i.e. $\theta = 90°$, vertical pipe). The two momentum balance equations (Eqns. (84) and (85)) are solved numerically for pressure gradient and dimensionless film thickness (δ/d). However, the solution of these two equations inquires obtaining of interfacial shear stress and film shear stress, which in their turn requires calculations of core gas and liquid film velocities. The step-by-step calculation procedure of τ_i and τ_F is presented in next section.

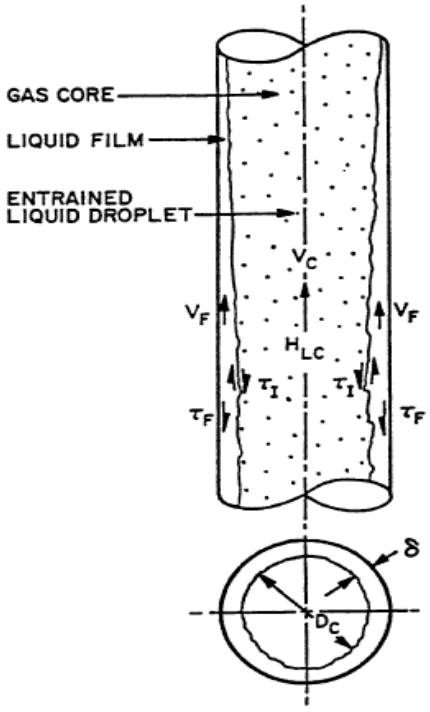

Figure 2.14 Schematic of annular flow in a pipe (Ansari et al. 1994)

For the sake of simplicity, the gas core with liquid droplets is treated as homogenous fluid with the assumption of no-slip velocity between gas and liquid (i.e. gas and entrained liquid droplets flow at the same velocity). Thus, the density of core gas is calculated as follows:

$$\rho_c = \rho_c \lambda_{LC} + \rho_g (1 - \lambda_{LC}) \tag{86}$$

where λ_{LC} is in-situ liquid holdup in the gas core, and is given by:

$$\lambda_{LC} = \frac{F_E v_{SL}}{v_{Sg} + F_E v_{SL}} \tag{87}$$

F_E is the fraction of the total liquid entrained in the core, proposed by Wallis (1969) as:

$$F_E = 1 - exp[-0.125(v_{crit} - 1.5)] \tag{88}$$

where

$$v_{crit} = 10000 \frac{v_{Sg} \mu_g}{\sigma_L} \left(\frac{\rho_g}{\rho_L}\right)^{0.5} \tag{89}$$

As in the annular flow pattern, the liquid film flows always upward along the pipe wall, and the shear stress, τ_F , is calculated from the following relationship as a function of in situ liquid film velocity, friction factor, liquid density:

$$\tau_F = f_F \rho_L \frac{v_F^2}{8} \tag{90}$$

f_F can be obtained from the Moody diagram or Eqn. (64) for a Reynolds number defined in Eqn. (91).

$$N_{Re_F} = \frac{\rho_L v_F d_{HF}}{\mu_L} \tag{91}$$

In Eqn. (91), determining a Reynolds number requires calculation of liquid film velocity and hydraulic film diameter, which are respectively given by:

$$v_F = \frac{q_{L\,(1-F_E)}}{A_F} = \frac{v_{SL(F_E)}}{4\underline{\delta}\,(1-\underline{\delta}\,)} \tag{92}$$

and

$$d_{HF} = 4\underline{\delta}\,(1-\underline{\delta}\,)d \tag{93}$$

Subsequently, τ_F becomes

$$\tau_F = \frac{f_F}{8}(1-F_E)^2 \rho_L \left[\frac{v_{SL}}{4\underline{\delta}\,(1-\underline{\delta}\,)d}\right]^2 \tag{94}$$

By simplifying Eqn. (94), it will reduce to:

$$\tau_F = \frac{d}{4}\frac{(1-F_E)^2}{4\left[4\underline{\delta}\,(1-\underline{\delta}\,)\right]^2}\frac{f_F}{f_{SL}}\left(\frac{dp}{dL}\right)_{SL} \tag{95}$$

In Eqn. (95), superficial liquid friction pressure gradient is calculated as:

$$\left(\frac{dp}{dL}\right)_{SL} = \frac{f_{SL}\rho_L\, v_{SL}^2}{2d} \tag{96}$$

where f_{SL} denotes the friction factor for superficial liquid velocity and can be obtained from the Moody chart or Eqn. (64) for a Reynolds number given by:

$$N_{Re_{SL}} = \frac{\rho_L v_{SL} d}{\mu_L} \tag{97}$$

The shear stress at the gas-liquid interface, which is shown in Eqns. (84) and (85), can be calculated by:

$$\tau_i = f_i \frac{\rho_c v_c^2 d}{8} \tag{98}$$

In Eqn. (98), ρ_c is core density, which can be obtained from Eqn. (86), v_c and f_i are core velocity and friction factor at the gas – liquid interface, which are given as following:

$$v_c = \frac{v_{SC}}{\left(1 - 2\underline{\delta}\right)^2} \tag{99}$$

and

$$f_i = f_{SC} Z \tag{100}$$

Z parameter is a correlating factor for interfacial friction factor and film thickness. Two equations for Z can be used, based on the performance of the model. The Wallis's Z expression which is good for thin film (Eqn. 101) and Whalley and Hewitt expression that works for thick film or low entrainment (Eqn. 102) and they are given by:

$$Z = 1 + 300\underline{\delta} \qquad for\ F_E > 0.9 \tag{101}$$

and

$$Z = 1 + 24\left(\frac{\rho_L}{\rho_g}\right)^{0.33} \underline{\delta} \qquad for\ F_E < 0.9 \tag{102}$$

By combining Eqns. (98) through (100) yields:

$$\tau_i = \frac{d}{4} \frac{Z}{\left(1 - 2\underline{\delta}\right)^4} \left(\frac{dp}{dL}\right)_{SC} \tag{103}$$

In Eqn. (103), the superficial friction pressure gradient in the core is expressed as

$$\left(\frac{dp}{dL}\right)_{SC} = \frac{f_{SC} \rho_c v_{SC}^2}{2d} \tag{104}$$

f_{SC} can be obtained from the Moody chart (Eqn. 64) for a Reynold number defined by:

$$N_{Re_{SC}} = \frac{\rho_c v_{SC} d}{\mu_{SC}} \tag{105}$$

where v_{SC} and μ_{SC} are superficial gas core velocity and gas core viscosity, which are given by Eqsn. (106) and (107):

$$v_{SC} = F_E v_{SL} + v_{Sg} \tag{106}$$

and

$$\mu_{SC} = \mu_C \lambda_{LC} + \mu_g (1 - \lambda_{LC}) \tag{107}$$

By substituting the above equations into equations (84) and (85), the pressure gradient at the gas-liquid interface and at liquid film can be calculated as:

$$\left(\frac{dp}{dL}\right)_c = \frac{Z}{\left(1 - 2\underline{\delta}\right)^5}\left(\frac{dp}{dL}\right)_{SC} + \rho_c g sin\theta \tag{108}$$

and

$$\left(\frac{dp}{dL}\right)_F = \frac{(1-F_E)^2}{64\underline{\delta}^3\left(1-2\underline{\delta}\right)^3}\left(\frac{f_F}{f_{SL}}\right)\left(\frac{dp}{dL}\right)_{SL} - \frac{Z}{4\underline{\delta}(1-\underline{\delta})\left(1-2\underline{\delta}\right)^3}\left(\frac{dp}{dL}\right)_{SC} + \rho_L g sin\theta \tag{109}$$

Based on the model assumption, the pressure gradient at the two phases interface is equivalent to that one at the liquid film at the pipe wall. By equaling two equations (Eqns. (108) and (109) the following equation will be formulated:

$$\begin{aligned} &\frac{Z}{4\underline{\delta}\left(1-\underline{\delta}\right)\left(1-2\underline{\delta}\right)^5}\left(\frac{dp}{dL}\right)_{SC} - (\rho_L - \rho_c) g sin\theta \\ &\qquad - \frac{(1-F_E)^2}{64\underline{\delta}^3\left(1-2\underline{\delta}\right)^3}\left(\frac{f_F}{f_{SL}}\right)\left(\frac{dp}{dL}\right)_{SL} = 0 \end{aligned} \tag{110}$$

In Eqns. (96) through (110), the dimensionless film thickness $\underline{\delta}$ is the only unknown parameter. Therefore, in this study, the bisection method was applied in order to determine $\underline{\delta}$. Once dimensionless film thickness is obtained, then the film thickness can be simply calculated, and total pressure gradient can be calculated using Eqn. (108) or (109). Finally, the total pressure gradient, which incorporated the acceleration component at high velocity, is given by (Hasan and Kabir 1988):

$$\left(\frac{dp}{dl}\right)_T = \frac{\left(\frac{dp}{dl}\right)_e + \left(\frac{dp}{dl}\right)_f}{\left[1 - \left(\rho_c v_g^2 / P\right)\right]} \tag{111}$$

Figure 2.15 shows the overall solution flow chart for the annular flow model.

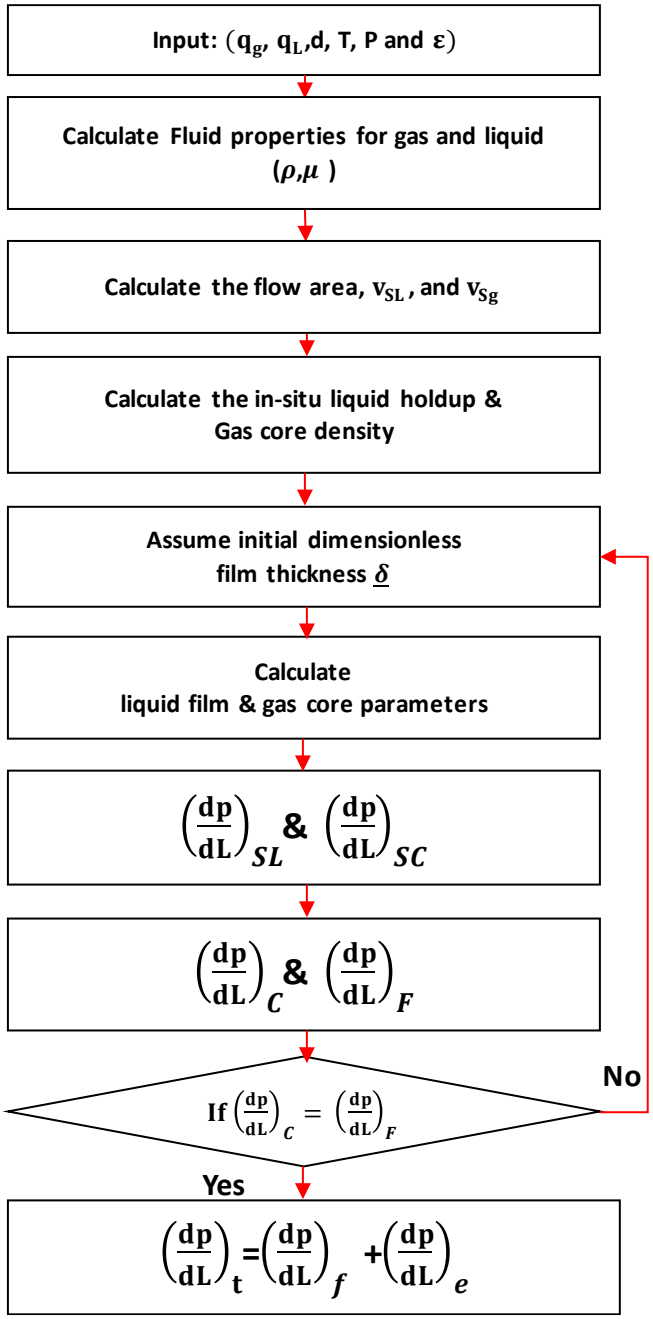

Figure 2.15 Flow chart for annular-flow calculation

2.8.2.5 Hybrid Model

In this study, the WCD model was extensively tested by randomly simulating various reservoir parameters, wellbore conditions, fluid properties, and surface conditions. Under some conditions, it was observed that the model failed due to exaggeration in the pressure gradient prediction in one of the grids. The dramatic change in the pressure gradient prediction occurs due to a quick change in the flow pattern that in its turn causes instability in the numerical calculation process incorporated in the nodal analysis model. Thus, a new hybrid mechanistic model was developed to overcome the quick transition between the flow patterns and ensure a

smooth transition. In the WCD model formulation, two hybrid models were incorporated for accurately predicting pressure gradient. The model limitation is quantified based on the superficial gas velocity value. The models are i) hybrid model for low and high velocities slug (V_{sg} = 2 – 6 m/s); and ii) hybrid model for annular and high-velocity slug (V_{sg} = 15 – 25 m/s), as shown in **Figure 2.9**. In the hybrid models, the total pressure gradient is calculated using the weighted average method. For instance, pressure gradient obtained from the hybrid model for low and high velocities slug is given by:

$$\left(\frac{dp}{dL}\right)_{Hyb} = \left(\frac{V_{sg\_T} - V_{sg\_Lower}}{V_{sg\_Upper} - V_{sg\_Lower}}\right)\left(\frac{dp}{dL}\right)_{LS} + \left(\frac{V_{sg\_Upper} - V_{sg\_T}}{V_{sg\_Upper} - V_{sg\_Lower}}\right)\left(\frac{dp}{dL}\right)_{HS} \quad (112)$$

where V_{sg_Lower}= 2 m/s and V_{sg_Upper} = 6 m/s

For annular – high-velocity slug hybrid model, the total pressure gradient is calculated as:

$$\left(\frac{dp}{dL}\right)_{Hyb} = \left(\frac{V_{sg\_T} - V_{sg\_Lower}}{V_{sg\_Upper} - V_{sg\_Lower}}\right)\left(\frac{dp}{dL}\right)_{HS} + \left(\frac{V_{sg\_Upper} - V_{sg\_T}}{V_{sg\_Upper} - V_{sg\_Lower}}\right)\left(\frac{dp}{dL}\right)_{Ann} \quad (113)$$

where V_{sg_Lower}= 15 m/s and V_{sg_Upper} = 25 m/s. $\left(\frac{dp}{dL}\right)_{Hyb}$ is the total pressure gradient calculated from the hybrid model, $\left(\frac{dp}{dL}\right)_{LS}$, $\left(\frac{dp}{dL}\right)_{HS}$, $\left(\frac{dp}{dL}\right)_{Ann}$ are the total pressure gradient calculated from low-velocity slug, High-velocity slug, and annular flow model, respectively. V_{sg_Lower} and V_{sg_Upper} are the lower and upper superficial gas velocities boundary for each hybrid model. V_{sg_T} is the test superficial gas velocity.

2.8.2.6 Sonic Condition Determination Model

The new model developed in this study, combines the two existing models from Kieffer (1977) and Wilson and Roy (2008) which were validated by the static two-phase mixture experiments. It combines the models presented in two studies. It is validated with data from two-phase flow experiments at OU. The comparative analysis of simulated sonic model and experimental data from OU flow loop shows reasonable agreement.

The new model predicts the sonic velocity based on the volumetric gas fraction and upstream pressure. The calculated sonic velocity acts as the criterion for sonic boundary. The fluid velocity for each grid is compared with the calculated sonic velocity for that grid. Whenever, the sonic velocity matches with the fluid velocity in that grid, the sonic condition establishes in the wellbore section. After that the flow decouples from the previous grid and the flow is limited by the sonic condition, where the well flow pressure is calculated using the sonic velocity.
Below is the model for prediction of velocity of sound in two-phase flow. It is divided in two cases.

Case 1: Upstream pressure less than 100 bar.

$a_1 = 80.44$
$a_2 = -0.0607$
$a_3 = 30.52$
$b_1 = 0.6337$
$b_2 = 23.23$
$b_3 = 0.672$
$c_2 = 74.42$

$$V_{sound} = (a_1 P^{b1})x^2 - (a_2 P^2 + b_2 P + c_2)x + a_3 P^{b3} + 20 \quad (114)$$

Case 2: Upstream pressure greater than 100 bar

$a_1 = 1800$
$a_2 = -0.0002878$
$a_3 = 220.4$
$b_1 = -0.01989$
$b_2 = 0.8032$
$b_3 = 0.2486$
$c_2 = 1884$

$$V_{sound} = (a_1 P^{b1})x^2 - (a_2 P^2 + b_2 P + c_2)x + a_3 P^{b3} + 20 \quad (115)$$

where P is the pressure in bar; V_{sound} is the velocity of sound in m/s; a_1, a_2, a_3, b_1, b_2, b_3, and c_2 are constants; and x is volumetric fraction of gas given by the following formula:

$$x = \frac{v_{Sg}}{v_{Sg} + v_{SL}}$$

where v_{Sg} is the superficial gas velocity and v_{SL} is the superficial liquid velocity. Figure 2.16 shows the comparison of experimental result and predicted value of sonic velocity using the developed model.

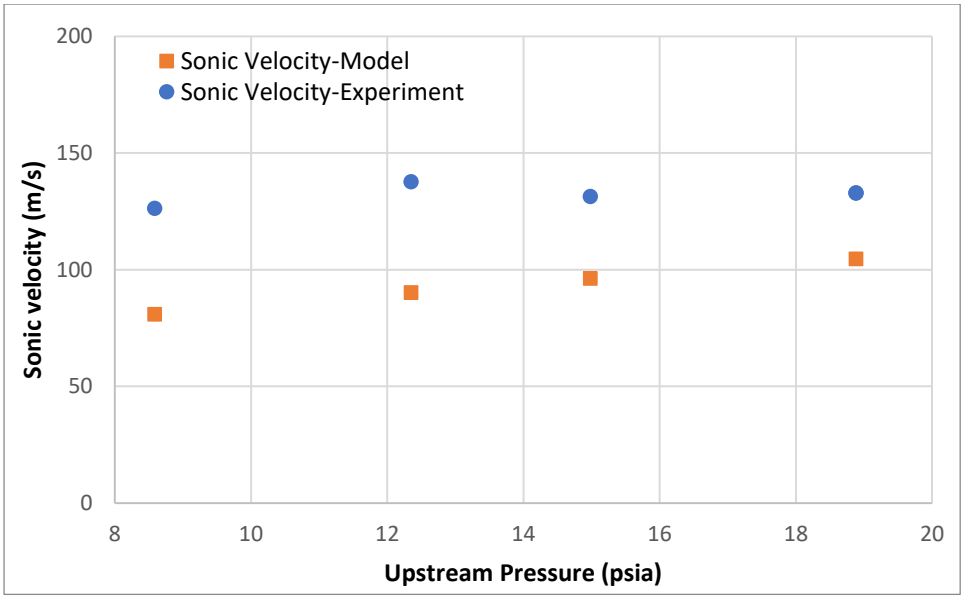

Figure 2.16 Comparison of sonic velocity from model and OU experimental data with respect to upstream pressure

2.9 Validation of Fluid Flow Models

During this project study, one of the key findings is that accurate prediction of WCD scenario is strongly related to the accuracy of single and two-phase flow model. Therefore, the accuracy of various mechanistic models, which were incorporated in the WCD tool for pressure gradient prediction in the wellbore, was extensively evaluated. The evaluation was conducted by comparing the pressure gradient predictions with the experimental measurement obtained from OU laboratory study and other existing studies. The comparison was carried out under a wide range of superficial gas and liquid velocities, pipe size, and inclination angle. For high gas and liquid flowrate, the experimental data was acquired from the multiphase flow loop in the Well Construction Technology Centre of University of Oklahoma. However, the experimental data for low gas and liquid flowrates was acquired from the literature. The measurements were used to validate the WCD model.

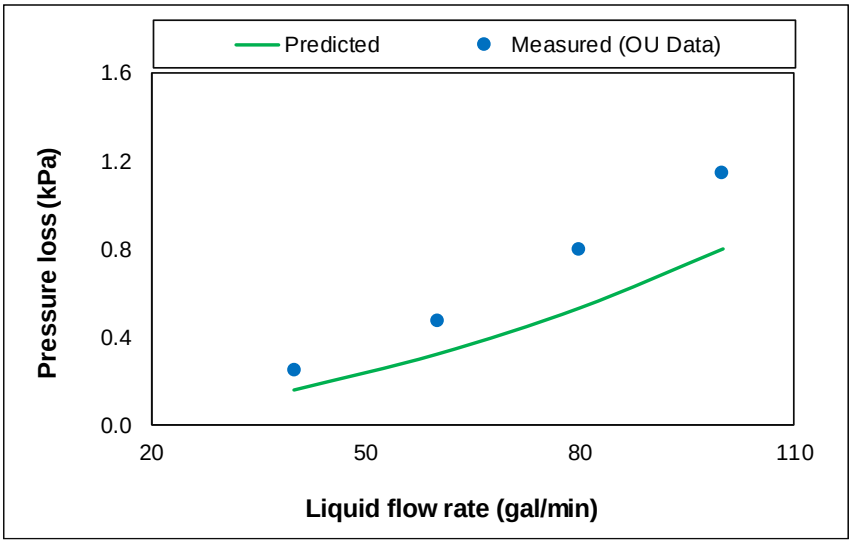

Figure 2.17 Comparison between measured and calculated pressure drop in a vertical pipe

The single-phase experiments were performed by circulating water at an ambient temperature varying flow rate (40 - 100 gpm). The test section is an insulated stainless pipe of 83 mm in diameter and 6.7 meters in length. The pressure drop measurements obtained from the experiment were compared with the predicted pressure drop model in a circular pipe, which is shown in **Figure 2.17**. Chen 1979 equation for friction factor was used in the calculation. Pressure loss (ΔP) in any circular duct is related to diameter (D), length (L), fluid density (ρ) and mean fluid velocity (V). Thus:

$$\Delta P = f\frac{2L}{D}\rho V^2 \tag{116}$$

where f is the fanning friction factor. In this analysis, L is the distance between pressure transducer ports. The friction factor used in the calculation of pressure loss is expressed as (Chen, 1979):

$$\frac{1}{\sqrt{f_D}} = -2.0\ log\left[\frac{\varepsilon}{3.7065D} - log\left(\frac{1}{2.8257}\left(\frac{\varepsilon}{D}\right)^{1.1098} + \frac{5.8506}{R_e^{0.8981}}\right)\right] \tag{117}$$

where f_D is the Darcy friction factor, which is defined as four-fold of the Fanning friction factor. ε is the pipe roughness, R_e is the Reynold number. The importance of this comparison is to validate the accuracy of the experimental measurement.

Two-phase flow mechanistic models were developed in the University of Oklahoma to predict pressure gradient and WCD. These models are validated using the data from the experiments obtained from the multiphase flow laboratory in WCTC and other investigators. The test section in which the experiments were carried out is an insulated stainless pipe of 83 mm in diameter and 6.7 meters in length and liquid and gas superficial velocities range are 0.06-2.9 m/s and 6-

165 m/s respectively. The validations for slug and annular flows are presented in **Figs. 2.18** and **2.19**, respectively.

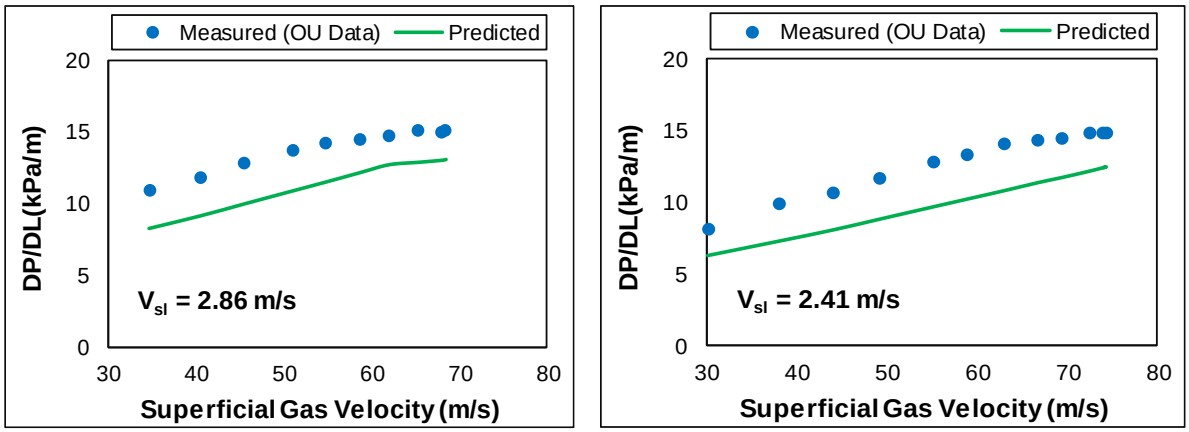

Figure 2.18 Comparison of measured and predicted pressure gradient for slug flow at two different superficial liquid velocities

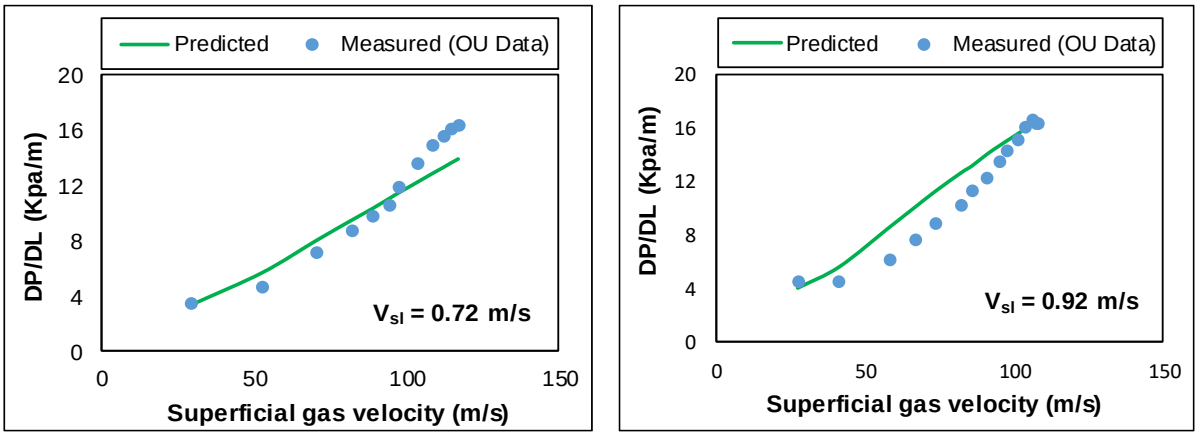

Figure 2.19 Comparison of measured and predicted pressure gradient for annular flow at two different superficial liquid velocities

For large pipe diameter (8 and 12 in), the two-phase flow mechanistic model predictions were validated with experimental data obtained from Ohnuki & Akimoto (2000) and Waltrich et al. (2015) at range of 0.18 – 1.06 m/s superficial liquid velocity and 0.03 – 8 m/s superficial gas velocity. The comparison between model predictions and measurement data for 8 and 12 in is shown in **Figures 2.20** and **2.21**, respectively. As displayed in the figures, a good agreement was obtained between the predicted and measured pressure gradient with discrepancy less than 18%. This accuracy in the pressure gradient prediction reveals the reliability and strength of the developed WCD computational tool.

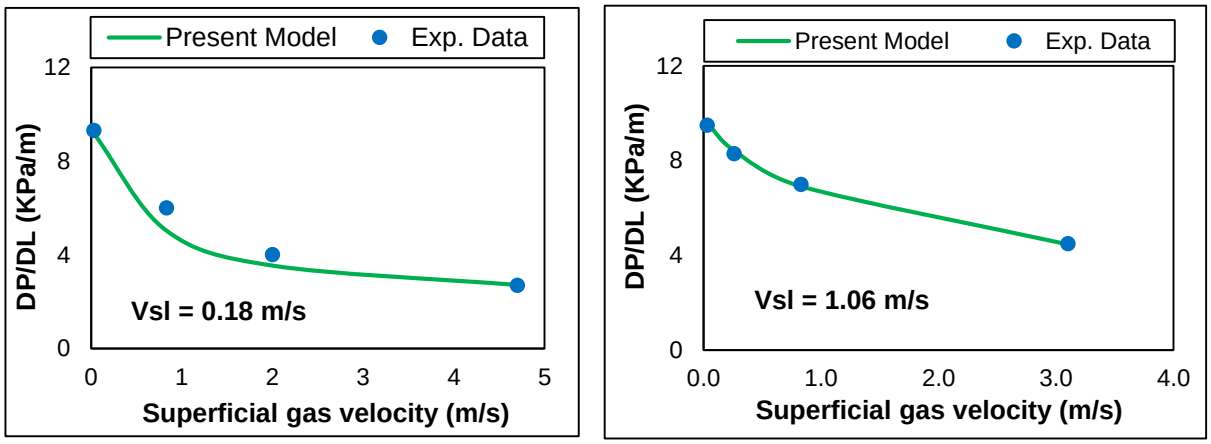

Figure 2.20 Comparison of measured and predicted pressure gradient in 8 in a vertical pipe (experimental data obtained from Ohnuki & Akimoto 2000)

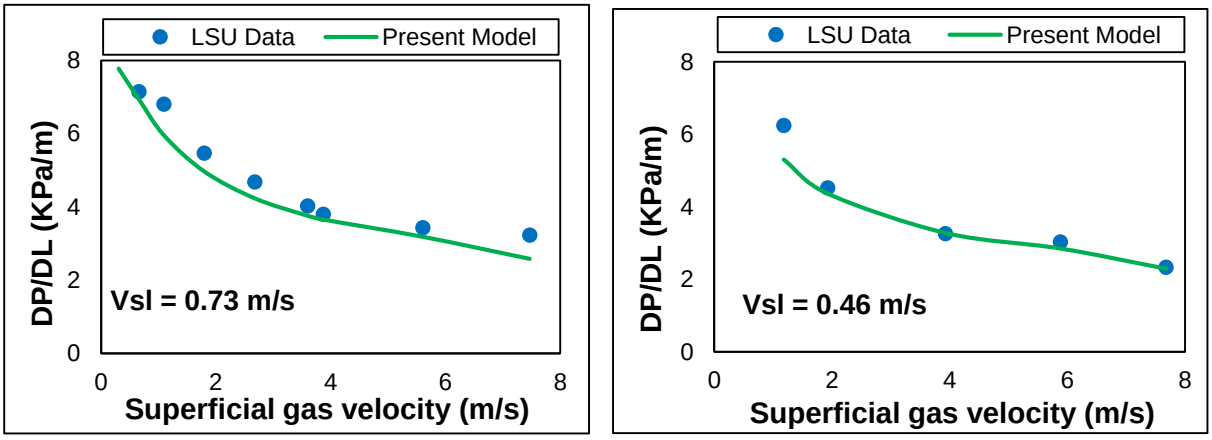

Figure 2.21 Comparison of measured and predicted pressure gradient in 12 in a vertical pipe (experimental data obtained from Waltrich et al. 2015)

With respect for the inclination angle effect, our model predictions of pressure gradient are validated with existing experimental data developed by Perez (2008) at different pipe inclination angles range from 30 to 90°. It is noteworthy that the inclination angle in his experiment was measured from the horizontal level ($\theta = 90$ refers to vertical position). The comparison was carried out using different pipe size and a wide range of superficial gas velocity, as shown in **Figures 2.22** and **2.23.** As depicted from the figures, an acceptable agreement was observed between the measured and predicted pressure gradient. The discrepancy is obtained to be less than 30%. It should be noted that Perez's data was obtained at relatively low superficial gas velocity. Due to lack of pressure gradient measurement for the inclined pipe at high superficial gas velocity, we were not able to assess the model performance at high flow conditions. The only pressure gradient for the inclined section was reported by Luo et al. (2016). However, the comparison was not performed due to the missing test pressure measurement that is considered as one of the key input data for high-pressure two-phase flow mechanistic model.

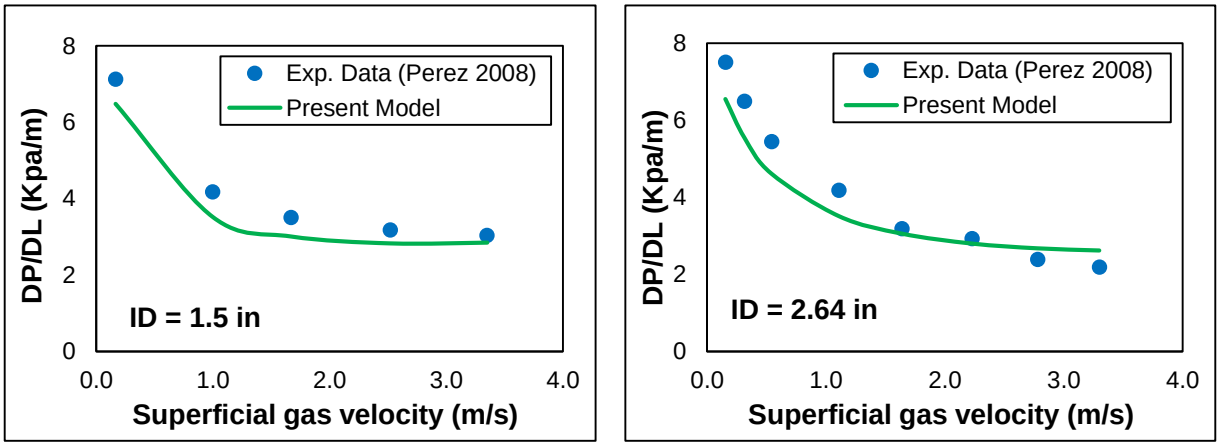

Figure 2.22 Comparison of measured and predicted pressure gradient for low superficial gas velocity at 30° inclination angle from the vertical

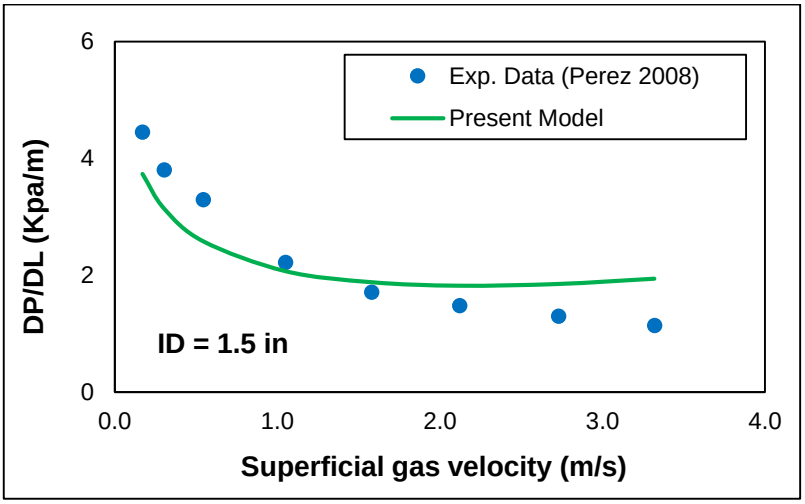

Figure 2.23 Comparison of measured and predicted pressure gradient in the inclined pipe at 60° from the vertical

2.9.1 Mean Percentage Error

Evaluation of WCD tool is carried out by comparing the measured pressure gradient with the pressure gradient from the WCD tool. The evaluation of the WCD tool using experimental data acquired is based on the statistics tool (Eqn. 118). Table 2.3 depicts mean percentage error for Figures 2.18 and 2.19.

$$E = \left(\frac{\Delta P/\Delta L_{predicted} - \Delta P/\Delta L_{Measured}}{\Delta P/\Delta L_{Measured}} \right) * 100 \tag{118}$$

$$MPE = \frac{1}{n} \sum_{i-1}^{n} /E/ \tag{119}$$

where MPE is mean percentage error

Table 2.3: Comparison of measured and predicted pressure gradient

V_{SL} (m/s)	Flow pattern	Mean Percentage Error (%)
2.86	Slug	-18.45
2.41	Slug	-21.49
0.95	Annular	22.79
0.72	Annular	20.51

3. Conclusions

This report presents various models incorporated to develop a Worst-Case Discharge (WCD) tool. The WCD tool can predict the pressure profile along the wellbore, flow patterns and also calculate the Worst-Case Discharge rate. Each model employed in the tool development was validated with experimental data. The high gas and liquid flowrate experimental data was acquired from the multiphase flow loop in Well Construction Technology Centre of the Department of Petroleum Engineering University of Oklahoma. However, the experimental data for low gas and liquid flowrate was acquired from the literature. Experimental data from both sources were used to validate the WCD model. The followings are the outcomes of this study:

- A sophisticated and accurate WCD – computational tool is developed to predict the daily uncontrolled flow of hydrocarbons from all producible reservoirs into open wellbore.
- The developed WCD tool consists of PVT model, reservoir performance model, production model, and hydrodynamic flow model. It provides satisfactory pressure gradient prediction in slightly deviated wells with inclination angle up to 45°.
- The tool accounts for the variety of reservoir types and produced fluid types as well as various wellbore configurations. It incorporates up to 15 reservoir layers with different characteristics and production rates.
- In addition to pressure profile prediction, WCD tool predicts superficial gas and liquid velocities, surface pressure and various flow patterns along the wellbore. It also highlights the occurrence of the sonic condition.
- The modified mechanistic model for pressure gradient (high-velocity slug and annular) incorporated in the WCD tool was validated with experimental pressure gradient data from OU flow loop. The predicted pressure gradients are in good agreement with the measured pressure gradient.
- Also, the predicted pressure gradient for large pipes (8 and12 in) is in in good agreement with the measured pressure gradient. The experimental data for the validation was obtained from literature.
- Sonic velocity is predicted as a function of upstream pressure and void fraction using existing models. As a result, good agreement was observed between predicted and measured sonic velocity under OU – lab test conditions.

References

Al-Shammasi, A. A. 2001. “A Review of Bubble-Point Pressure and Oil Formation Volume Factor Correlations” SPE Res Eval & Eng 4 (2): 146-160. SPE-71302-PA. http://dx.doi.org/10.2118/71302-PA

Ahmed, T. (2006). “Reservoir Engineering Handbook”. Third Edition

Ansari, A. M., Sylvester, N. D., Sarica, C., Shoham, O and Brill, J. P. (1994). “A Comprehensive Mechanistic Model for Upward Two-Phase Flow in Wellbores” Society of Petroleum Engineer Production & Facilities. pp. 143-152.

Beggs, H. D. and Robinson, J. R., (1975). “Estimating the Viscosity of Crude Oil Systems” Journal of Petroleum Technology. pp. 1140–1141.

Brotz,W. (1954). “Uber die Vorausberechnung der Absorptionsgesch-windig-keit von Gasen in Stromenden Flussigkeitsschichten" Chern. Ing. Tech.

Elsharkawy, A. M., and Alikhan, A. A. (1996). “Correlation for Predicting Solution Gas/Oil Ratio, Oil Formation Volume Factor, and Under Saturated Oil Compressibility” Journal of Petroleum Science and Engineering. pp 291-302

Fernandes, R.C., Semait, T., and Dukler, A.E. (1983) “Hydrodynamic Model for Gas-Liquid Slug Flow in Vertical Tubes”, AIChE J. Vol 29, No 6, pp. 981-989.

Frashad, F., LeBlanc, J.L., Garber, J.D. et al. 1996. “Empirical PVT Correlations for Colombian Crude Oils”. Presented at the SPE Latin American and Caribbean Petroleum Engineering Conference, Port of Spain, Trinidad and Tobago, 23–26 April. SPE-36105-MS. http://dx.doi.org/10.2118/36105-MS

Glaso, O., (1980) “Generalized Pressure-Volume-Temperature Correlations” Journal of Petroleum Technology, pp. 785–795.

Griffith, P. and Snyder, G. A. (1964). “The Bubbly-Slug Transition in a High Velocity Two-Phase Flow” Report No: 5003-29 (TID 20947) MIT, Cambridge.

Hasan, A. R., and Kabir, C.S. (1988). “A Study of Multiphase Flow Behavior in Vertical Wells”. Society of Petroleum Engineer Production Engineering.

Kieffer, S.W. 1977. Sound Speed in Liquid-gas Mixtures: Water-air and Water-steam. Journal of Geophysical research, 82(20), pp.2895-2904.

McCain, W. D (1990). “Petroleum Fluid”. Second Edition.

Luo, W., Li Y., Qinghua, W., Li J., Liao, R., & Liu, Z. 2016. Experimental Study of GasLiquid Two-Phase Flow for High Velocity in Inclined Medium Size Tube and Verification of Pressure Calculation Methods, international journal of heat and technology, 34, (3): 455-464.

Ohnuki, A., Akimoto, H., 2000. “Experimental Study on Transition of Flow Pattern and Phase Distribution in Upward Air–Water Two-Phase Flow along a Large Vertical Pipe”. Int. J. Multiphase Flow 26, 367–386

Perez, V. H. (2008). “Gas-liquid Two-Phase Flow in Inclined Pipes”. PhD Thesis, University of Nottingham. London, United Kingdom.

Shoham, O. (2005). “Mechanistic Modeling of Gas-Liquid Two-Phase Flow in Pipes” The Society of Petroleum Engineer.

Tengesdal, J. O., Sarica, C., Scmidt., Z., and Doty., D. (1999). “A Mechanistic Model for Predicting Pressure Drop in Vertical Two-Phaes Flow” Journal of Energy Resources Technology. ASME Vol 121, pp 1-8.

Torcaso, M. A., and Wyllie, M. R. J., (1958) “A Comparison of Calculated krg/kro Ratios with Field Data,” Journal of Petroleum Technology. pp. 6-57.

Vo, D.T. and Shoham, O. (1989). “A Note on the Existence of a Solution for Two-Phase Slug Flow in Vertical Pipe” ASME Journal of Energy Resources Tech. Vol 111, No 64, pp. 64-65

Wallis, G. B. (1969). One Dimensional Two-Phase Flow. McGraw-Hills Book Co. inc, New York.

Waltrich, P. J., Hughes R., Tyagi M., Kam S., Williams W., Cavalcanti de Sousa P. Zulqarnain M., Lee W., & Capovilla S. M. (2015). “Experimental Investigation of Two-Phase Flows in Large-Diameter Pipes and Evaluation of Flow Models Applied to Worst-Case- Discharge Calculations” BOEM Report M15PC00007, Craft & Hawkins Department of Petroleum Engineering, Louisiana State University, Baton Rouge.

Whalley, P. B., and Hewitt, G. F. (1978). “The Correlation of Liquid Entrainment Fraction and Entrainment Rate in Annular Two-Phase Flow” UKAEA. Report AERE-R9187, Harwell.

Wilson, P.S. and Roy, R.A., 2008. An audible demonstration of the speed of sound in bubbly liquids. American Journal of Physics, 76(10), pp.975-981.